Univerzita Karlova v Praze
Matematicko-fyzikální fakulta

DIPLOMOVÁ PRÁCE

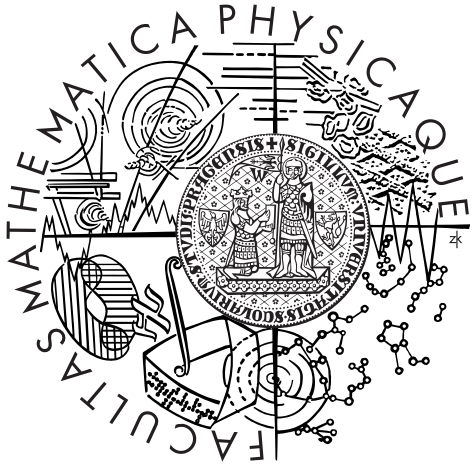

Robert Filgas

Výzkum blazarů metodou barevných indexů

Astronomický ústav Univerzity Karlovy

Vedoucí diplomové práce:
RNDr. René Hudec, CSc.

Studijní program:
fyzika

Studijní obor:
astronomie a astrofyzika

Při vypracování této diplomové práce mi tou největší měrou pomohli a na jejích kvalitních stránkách se podíleli vedoucí mé diplomové práce RNDr. René Hudec z ASÚ AV ČR, RNDr. Vojtěch Šimon z ASÚ AV ČR a doktorandi Milan Bašta a Martin Topinka. Děkuji jim za čas, který strávili zodpovídáním mých dotazů a za velmi cenné rady a konzultace, které mi vždy s ochotou poskytli.

Dále děkuji profesoru Alanu Marscherovi z Boston Univerzity a docentu Petru Harmancovi z Astronomického ústavu UK Praha za velmi přínosné rady a ochotu, s kterou mi je poskytli. Za pomoc s obstaráním fotometrických dat velice děkuji svému spolužákovi Jakubovi Řípovi. Za pomoc se záležitostmi ohledně programů pro zpracování textu a grafů děkuji Mgr. Michalu Švandovi a Dr. Ladislavu Šubrovi. Michalovi rovněž děkuji za cenné rady a pomoc s přípravou diplomové prezentace.

K úspěšnému řešení úkolů v rámci této práce přispěla i má činnost pomocné vědecké síly ve skupině Astrofyziky vysokých energií stelárního oddělení ASÚ AV ČR v Ondřejově, rád bych proto poděkoval ASÚ AV ČR za tuto podporu, jakožto i všem z ASÚ MFF UK.

Všem těmto, jakožto i mé rodině a přítelkyni děkuji za podporu a pomoc při psaní této diplomové práce. Touto cestou děkuji i těm, které jsem nezmínil a kteří mi také pomohli.

Jakékoliv případné chybné, nepřesné a nekvalitní údaje, uvedené v této diplomové práci, nemají s výše zmíněnými osobami a zdroji nic společného.

Prohlašuji, že jsem svou diplomovou práci napsal samostatně a výhradně s použitím citovaných pramenů. Souhlasím se zapůjčováním práce.

V Praze dne 15. dubna 2006 Robert Filgas

Contents

Název práce: Výzkum blazarů metodou barevných indexů
Autor: Robert Filgas
Katedra: Astronomický ústav Univerzity Karlovy
Vedoucí diplomové práce: RNDr. René Hudec, CSc., AÚ AV ČR
e-mail vedoucího: rhudec@asu.cas.cz
Abstrakt: Blazary představují fyzikálně důležitý případ aktivních galaktických jader, AGN. Projevují prudkou aktivitu a proměnnost na širokých škálách energií a časů a jsou jasné a vysokoenergetické zdroje. Zkoumáním blazarů můžeme studovat a analyzovat procesy vzniku vysokoenergetických fotonů. V této práci se věnujeme originálnímu přístupu ke studiu blazarů s důrazem na detailní barevné a spektrální analýzy s důsledky, které potvrzují analýzu barev jako účinný nástroj ke zkoumání prostředí objektů a možnost detekce kandidátů na blazary v celooblohových přehlídkách. Barevné indexy blazarů byly shledány podobné těm u optických dosvitů gama záblesků, což potvrzuje podobnost fyzikálních procesů tvořících optické záření (synchrotronové spektrum). Rozptyl barevných indexů zkoumaných blazarů je malý, proto prach podél zorné přímky (tj. ve výtrysku) byl pravděpodobně zničen energetickým zářením. Rozptyl AGN v barevném diagramu je značně větší než u blazarů, patrně proto, že zorná přímka není shodná s výtryskem, takže světlo je ovlivněno materiálem kolem AGN. To je ve shodě s obecným chápáním blazarů a AGN. Výsledky jsou diskutovány, včetně návrhů na budoucí práce.
Klíčová slova: AGN - blazar - barevný index - spektrální index

Title: Study of blazars using color indices
Author: Robert Filgas
Department: Astronomical Institute of Charles University
Supervisor: RNDr. René Hudec, CSc., AI AS CZ
Supervisor's e-mail address: rhudec@asu.cas.cz
Abstract: Blazars represent physically important case of Active Galactic Nuclei, AGN. They exhibit violent activity and variability over a wide range of energy and time and are luminous high-energy sources. Through investigation of blazars, processes of generation of high energy photons can be studied and analysed. In this study, we focus on novel approach of studies of blazars with focus on detailed colour and spectral analyses, with interesting consequences such as confirming the colour analyses as efficient tool for study the environment of the objects and/or possibility to detect blazar candidates in sky surveys. The colour indices of blazars were found to be similar to those of OA confirming similarity in physical processes generating the optical emission (synchrotron spectrum). The scatter of colour indices of analysed blazars is small and hence the dust along the line of sight i.e. in the jet was probably destroyed by energetic emission. The scatter in colour diagram of AGNs is significantly larger than those of blazars, probably because of the line of sight is not consistent with the jet, hence the light is affected by the material surrounding the AGN. This is consistent with the understanding of AGN and blazars in general. The results are discussed and suggestions for future prospects are drawn.
Keywords: AGN - blazar - color index - spectral index

1 Active galaxies

1.1 Introduction

There exist "normal" galaxies in the Universe and galaxies that are called AGN. The abbreviation AGN stands for Active Galactic Nuclei and suggests that inside these galaxies an "active" nucleus is present. This nucleus is seen in the spectra of AGN galaxies. Unlike normal galaxies whose spectra are mostly thermal, coming from the constituent stars in the galaxy, the spectra of AGN galaxies are non-thermal having origin in non-thermal processes. The AGN are usually very luminous and the theory assumes a black hole, typically of 10^7 to 10^9 solar masses, to be present in the center of an AGN galaxy. The surrounding matter, attracted by the gravitation of this massive black hole, is pulled towards it, forming an accretion disk, losing angular momentum through viscous and turbulent processes and spiraling down to the black hole. Frictional processes that take place during the fall of matter onto the black hole lead to the emergence of plasma emitting mainly in the UV and X-ray region. Clouds of gas in the vicinity of the black hole (either in BLR – broad line region – or in NLR – narrow line region) are excited and produce strong emission lines. BLR is situated closer to the black hole; the clouds move fast and emit broad lines. NLR is more extended; clouds of NLR move slower and emit narrow lines.

A dust torus is usually supposed to be present surrounding the black hole at the distance of about 1 pc and a jet of energetic particles is assumed to exist perpendicular to the dust torus, being responsible for the observed radio emission of some AGN (Antonucci 1993). Most of the luminosity of AGN is emitted in radio, IR, UV, X-ray and gamma-ray wavelengths rather than in the optical band.

1.2 Rarities of AGN

1.2.1 Strong emission lines

Observed emission lines are much broader than absorption lines so they might have been created at different places in different conditions. Broadness is generally caused by Doppler effect, gravitation, high temperatures or velocity. Positions of emission lines correspond to high excitation or ionization of atoms. It is possible to determine distance to the galaxy and its luminosity from observed redshift of lines and Hubble's law.

1.2.2 Variability of the luminosity

Variability of such giant objects as galaxies is really unexpected (perhaps except supernova explosion). Yet brightness of such object can increase thousand times on scale of days. The speed of this variability gives us an estimate of size, or better upper limit for dimensions, of area in which the change occurred. Variability cannot spread faster than the speed of light. From this we see that the active area is not larger than 1 parsec. However, it is just an estimate of radiating area, not an object which is the area part of.

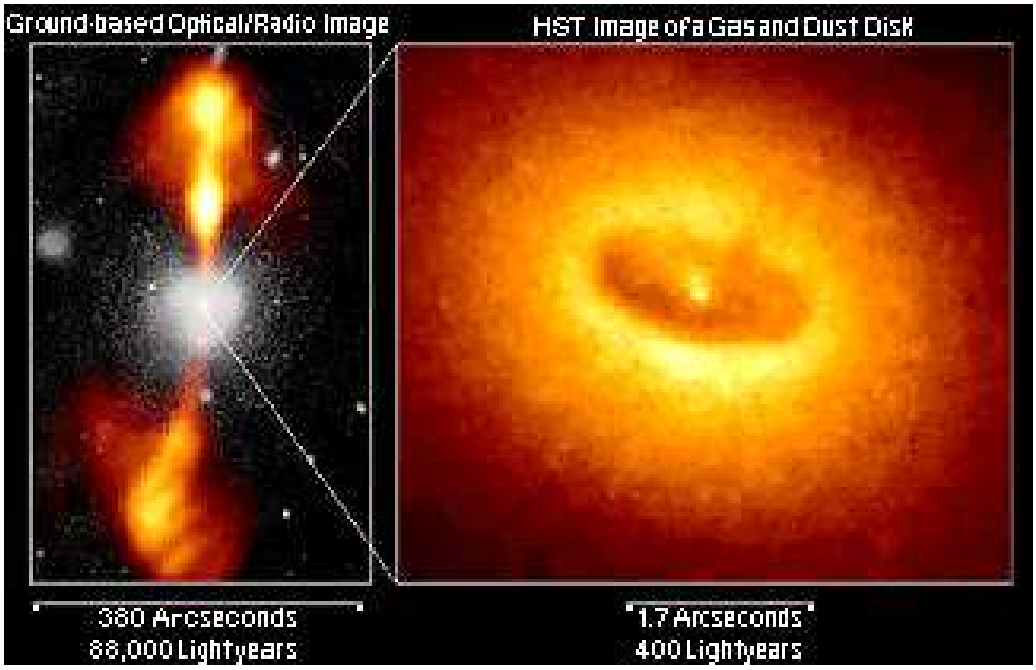

Figure 1: Photo of AGN NGC4261 by HST. (*Source:* NASA)

1.2.3 Differences in the spectrum

Observed electromagnetic spectrum of AGN is mostly very different from spectrum of absolute black body. The cause of this is large portion of non-thermal emission from radiation of the galaxy, caused by the presence of the active nuclei. Markedly represented here is synchrotron emission and also inverse Compton scattering.

1.3 Types of AGN

Nowadays different types of AGN are observed – radio galaxies, quasars, blazars, Seyfert galaxies, LINERs, nuclear H_{II} regions and starburst galaxies. This is a division from an observational point of view. However, in the unified model different classes of AGN (radio galaxies, quasars, blazars,...) are supposed to be intrinsically the same, all having the same environment outlined above. The observed variety of different types of AGN is just assumed to be a result of an orientation effect of the nuclei relative to the observer. Only the radio power of jets divides AGN intrinsically into radio loud and radio quiet ones. The former class has strong radio jets, whereas in the latter class the radio jets are weak.

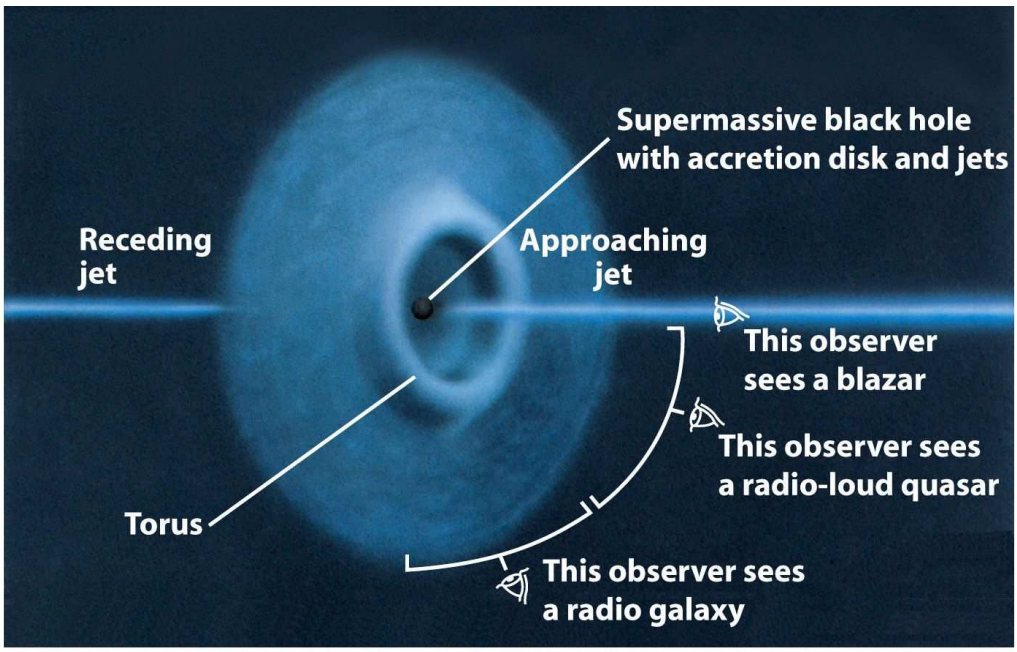

Figure 2: Schematics of AGN and how the type of object we observe depends on our point of view (*author*: Robert Antonucci)

1.3.1 Quasars

Word quasar is created from phrase quasi-stellar which means star-like object. Quasars are active galaxies and were discovered in the end of 1950s at the first radio maps of the sky. They were considered to be stars thence their name.

Their optical counterparts are very faint and it was not completely easy to identify them. The first identified source was 3C 48 (48th source of the third Cambridge catalogue of radio sources). However, obtaining object's

spectra revealed another questions. Continuum of the spectra contained broad emission lines which scientists were not able to match with lines of known elements. In 1962 astronomer Maarten Schmidt revealed in quasar 3C 273 Balmer series of hydrogen in position nobody would have look for. Cause of this effect was the cosmological redshift ($z = 0.16$ Nasa Extragactic Database).

Distances of quasars are billions of light years. They are therefore objects from the early period of the galaxy and universe evolution. Quasars no more occur in close surrounding. Black holes in the centers of galaxies like our Galaxy or galaxy in Andromeda have probably already consumed great part of the matter from their surrounding (Karas 1996). Later it was shown not only that not all quasars have strong radio emission but also that most of quasars (around 90 % (Kellermann et al. 1989)) radiate weakly in radio band of spectrum compared to optical band. Therefore we can distinguish radio-loud quasars (radiating strongly in radio band) from radio-quiet quasars (weak radio radiation). Strong radio emission which separates radio-loud and radio-quiet quasars is created by relativistic electrons moving in magnetic field in jets of radio-loud quasars. Spectra of quasars have a power-law shape from radio to optical band due to a strong non-thermal emission.

1.3.2 OVV quasars

Optically violently variable quasars are radio-loud quasars with continuous spectrum which has power-law shape to radio band and with strong emission lines. They differ from quasars by savage, very irregular brightness changes in optical and radio band. There are often years without sharp changes followed by sudden brightening of several magnitudes on scale of weeks or days (so-called outburst or flare). Besides, radiation is linearly polarized due to its synchrotron origin.

1.3.3 BL Lac type objects

It is a group of radio-loud objects named after its first representative BL Lacertae which was discovered in Lacerta constellation and marked as a variable star. BL Lac objects are highly variable in optical and radio wavelengths. They have continuous power-law spectrum to IR and radio band. Radiation is again strongly linearly polarized. These qualities would classify BL Lac objects as quasars, namely OVV quasar. The main difference between both is an absence of strong emission and absorption lines in optical spectrum of BL Lac objects. At first the lines were not observed at all but with improving technology it was possible to discover weak emission lines in optical spectrum shifted by redshift. Therefore extragalactic origin and affinity with quasars was confirmed.

1.3.4 Blazars

When the observer's line of sight is close to the direction of a powerful radio jet, a blazar is observed (name given by astronomer Ed Spiegel who during lunch at Pittsburgh conference in 1978 suggested that OVV quasars and BL Lac type objects had so much in common that they could form one class named blazars). Blazars appear point-like in the sky and have apparently a non-stellar continuum. Blazars usually have a compact core emitting at radio frequencies with a flat or inverted spectrum. They exhibit rapid (often flare-like) variability at all wavelengths (Ghisellini&Maraschi 1996, Villata et al. 2000) and a strong and variable optical polarization (Kollgaard et al. 1994, Urry&Padovani 1995, Ghisellini&Madau 1996). Periodicity of long-term brightness variability can be found in some blazars (Smith&Nair 1995, Raiteri et al. 2001). A relativistic jet is pointing almost towards us and the plasma in the jet is moving at relativistic speeds in the magnetic field. Hence superluminal motion, relativistic beaming and a very energetic emission at gamma frequencies are observed in many blazars.

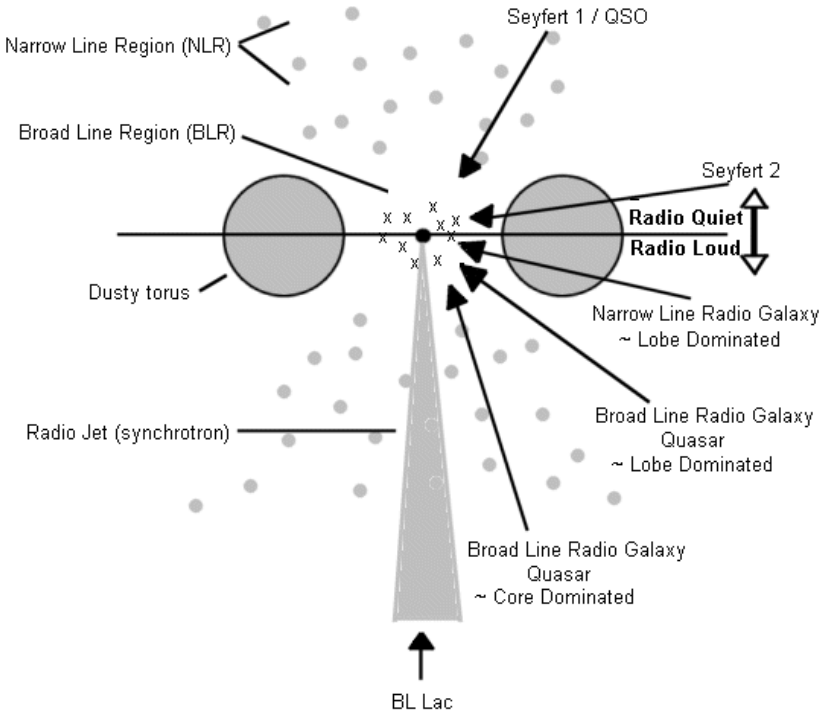

Figure 3: Schematic diagram for unified scheme of AGN (*Radomski* 2003)

1.4 Observational effects in jets of AGN

1.4.1 Superluminal motion

Superluminal motion describes proper motion of some source structure whose apparent speed projected to the sky is higher than the speed of light. This paradox was discovered by project VLBI (Very Long Baseline Interferometry), which measured distances of blobs in AGN jets from their cores. Due to time evolution of distance to the source it seemed that blobs are moving faster than light. The explanation lies in the geometry of this problem, because this phenomenon occurs when emitting regions are moving at very high speeds and for small viewing angles θ.

We can easily deduce relation between observed blob speed and their real speed (Karas 1996)

$$v_{\mathrm{app}} = \frac{v \sin\theta}{1 - \frac{v}{c}\cos\theta} \ . \tag{1}$$

Maximum v_{app} is for $\cos\theta = \frac{v}{c}$

When blob is created in the center of AGN, it radiates a signal towards us, which travels at the speed of light. When blob moves relativistically towards us and radiates again, then this signal travels to us from shorter distance and so it needs shorter time to reach the Earth than the first signal. In case we ignore this shift of the blob towards us, we observe tangential velocity of the blob even multiple times bigger than the speed of light.

1.4.2 Relativistic beaming

Relativistic beaming, on the other hand, strongly influences the luminosities. It is believed to explain rapid variations of luminosity, polarization, featureless continuum and high luminosities of blazars. As blazar jets are viewed at small angles their observed luminosity can be amplified by a factor of thousands. If we introduce Doppler factor as

$$\delta = \left[\gamma\left(1 - \frac{v}{c}\cos\theta\right)\right]^{-1} \tag{2}$$

then for a simple jet model where blobs are represented as spheres with relativistic speed and radiation synchrotron emission we get boosting of radiation intensity

$$L_{\mathrm{obs}} = \delta^{\mathrm{P}} L_{\mathrm{em}} \tag{3}$$

P equals $3 + \alpha$ for homogenous sphere, where α is a spectral index which describes power-law spectrum of synchrotron radiation and is defined as

$$F_\nu \sim \nu^{-\alpha} \tag{4}$$

However it is necessary to have a small angle between the jet and direction to the observer because Doppler factor is decreasing quickly for bigger angles.

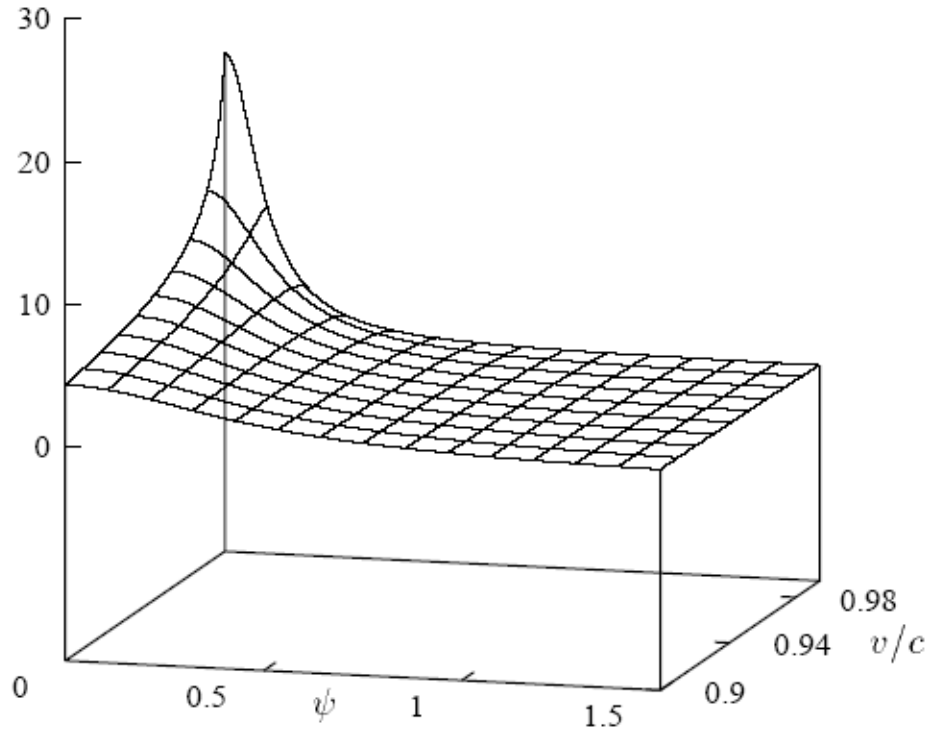

Figure 4: The Doppler factor δ as a function of a viewing angle ψ and speed v/c (*Karas* 1996)

Relativistic beaming can also explain why we for some AGN observe only one jet. While the jet which is pointing towards us is boosted by this effect, its counter-jet is by the same effect weakened so much that we do not detect it.

2 Spectra of blazars and their physical origin

2.1 Introduction

The non-thermal radiation from blazars usually outshines the emission of the host galaxy. The spectrum of blazars is the widest of all AGN. It extends from radio frequencies to highly energetic gamma-rays (TeV) and is characterized by two broad components. These components are generally ascribed to the synchrotron radiation for lower frequencies and the inverse Compton radiation for higher frequencies.

2.2 Synchrotron emission

If an electron moves in magnetic field, it is forced by the Lorentz power to spiral around magnetic line of force. Since this is an accelerated movement, the charged particle has to radiate the energy. Electrons give their energy in the form of photons with the wavelength proportional to the induction of the magnetic field. For classic electrons is this emission called cyclotron and is monochromatic. If the electrons move at relativistic speeds then it is called synchrotron emission. Its spectrum is continuous, spectral line corresponding to cyclotron emission of the same magnetic induction would broaden due to relativistic effects. Non-relativistic electron spirals with gyrofrequency (Karas 1996)

$$\omega_{\mathrm{L}} = \frac{|e|B}{m_{\mathrm{e}}} \tag{5}$$

with Larmor radius

$$r_{\mathrm{L}} = \frac{v_{\perp}}{\omega_{\mathrm{L}}} \tag{6}$$

Energy radiated by the electron increases as

$$(v_{\perp}B)^2 \tag{7}$$

Spectrum consists only from the frequency of circling electron.

m_{e} represents mass of the electron, e its charge, B its magnetic induction and $v_{\perp}$ component of the electron velocity in the plane perpendicular to $\boldsymbol{B}$ ($v_{\perp} = v \sin\alpha$ where α is an angle between $\boldsymbol{B}$ and $\boldsymbol{v}$).

Relativistic electron circling in the static magnetic field radiates the synchrotron emission in the direction of its movement with frequency shifted by Lorentz factor

$$\omega_{\mathrm{B}} = \frac{\omega_{\mathrm{L}}}{\gamma} \tag{8}$$

and with the radius

$$r_{\mathrm{B}} = \gamma\, r_{\mathrm{L}} \tag{9}$$

Radiated energy of one electron increases as

$$\gamma^2 \left(v_{\perp} B\right)^2 \tag{10}$$

Synchrotron emission is much stronger than the cyclotron one. The spectrum is broad and centered on a critical frequency ω_{c}

$$\omega_{\mathrm{c}} \sim \gamma^2 B \sim \gamma^2 \omega_{\mathrm{L}} \tag{11}$$

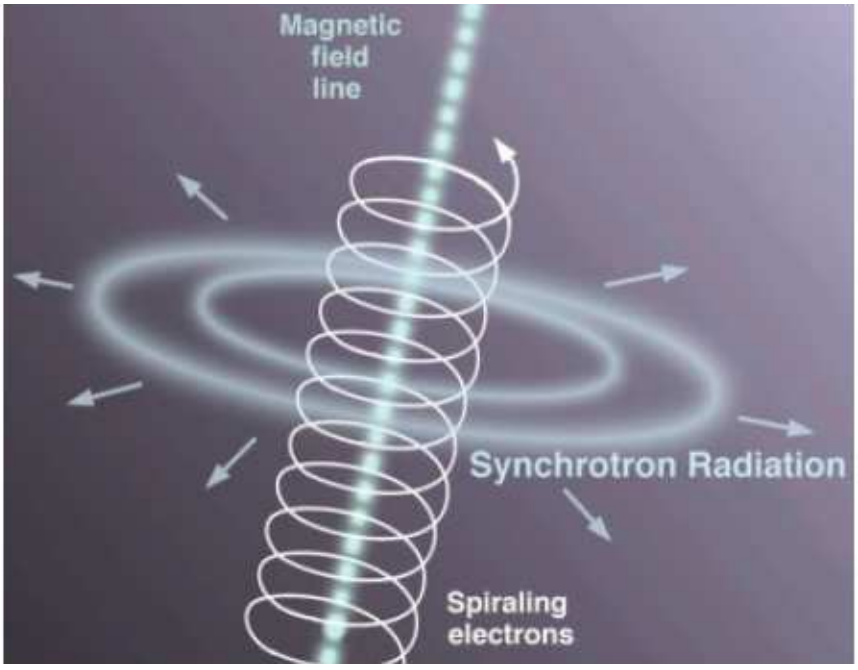

Figure 5: A schematic of synchrotron radiation (*illustration by Jon Lomberg; image credit: Gemini observatory*)

The nature of synchrotron spectrum depends on the speed of electrons. The energy distribution of electrons has a power-law nature and so the synchrotron spectrum is power-law as well.

Some of the radio synchrotron sources are so compact that they absorb their own radiation. That is why under certain frequency electrons are optically thick for their own radiation and so-called synchrotron self-absorption becomes apparent.

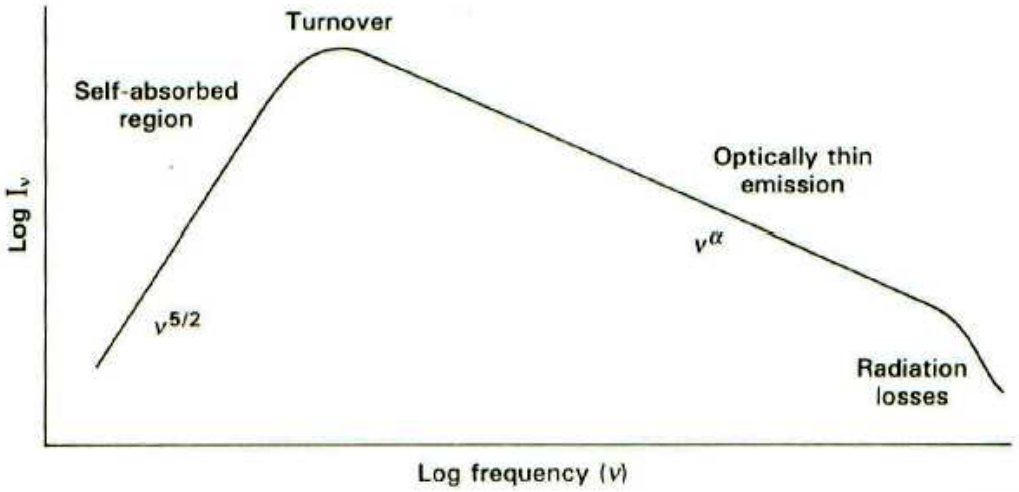

Figure 6: Synchrotron spectrum schematic (*Robson* 1996)

2.3 Inverse Compton scattering

When relativistic electrons interact with photons, energy of photons increases at the expense of kinetic energy of electrons. This is called inverse Compton scattering. This process is therefore a cooling mechanism for electrons and a source of high-energy photons. Energetic gain of photons from relativistic electrons is very high. The average energy of scattered photon for isotropic radiation can be expressed as

$$\langle E' \rangle = \frac{4}{3}\beta^2\gamma^2 E \tag{12}$$

This gives us the factor of energy increase $\frac{4}{3}\gamma^2$ for relativistic ($\beta \to 1$) electrons. Equations are the same as for the synchrotron emission so here too is the spectrum slope determined by the power-law.

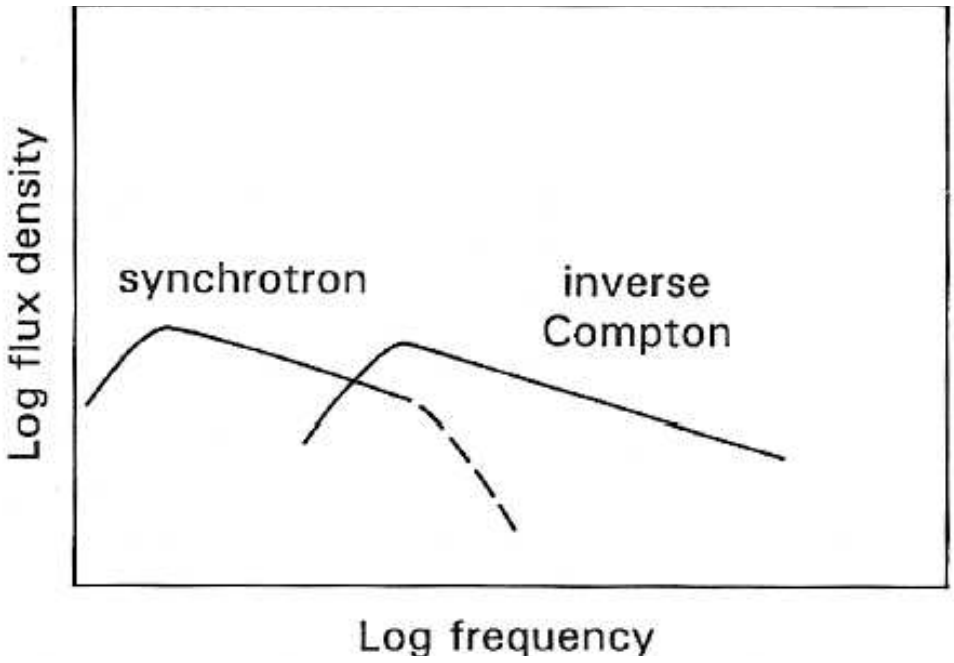

Figure 7: Synchrotron and inverse Compton spectrum in logarithmic scale (*Robson* 1996)

2.4 Classification of blazars by the spectrum shape

The blazar class includes Flat-Spectrum Radio Quasars (FSRQ) and BL Lacertae objects. These are thought to be the "beamed" counterparts of high- and low- luminosity radio galaxies, respectively. The main difference between the two blazar classes lies in their emission lines, which are strong and quasar-like for FSRQ and weak or in some cases outright absent in BL Lacs (Padovani 2003). It is useful to divide BL Lacs into High-frequency peaked BL Lacs (HBL) and Low-frequency peaked BL Lacs (LBL) (Padovani&Giommi 1995). These may indeed be opposite extremes of a continuous distribution because current BL Lac samples come from radio or X-ray surveys with fairly high flux limits and so are naturally dominated by LBL or HBL, respectively (Urry 1996). The strong emission-line blazars (FSRQ), also generally radio-selected, have continua like LBL (Sambruna et al. 1996). BL Lacs found in the first X-ray surveys were generally HBL; BL Lacs found in classical radio surveys were generally LBL, as were most FSRQ, though high-frequency FSRQ are now being identified in multiwavelength surveys designed not to exclude them (Perman et al. 1998). In any case, the spectral energy distributions of HBL and LBL/FSRQ differ in several ways. The peak wavelength of the synchrotron component is in the infrared-optical band for LBL and FSRQ, whereas it peaks in the extreme ultraviolet to soft X-ray range for HBL (see Fig. 8). Also, LBL and FSRQ have a higher ratio

of gamma-ray to synchrotron flux than the HBL (Sambruna et al. 1996).

Because of these systematic spectral differences, the observational details of the multiwavelength study dictate the type of blazar studied. To study blazars above the synchrotron peak, where they are most variable, means selecting UV- and X-ray-bright targets, which are inevitably HBL. To study correlated intraday variability at radio and optical wavelengths means selecting LBL/FSRQ. With higher sensitivities, this artificial distinction will disappear, but as observed, the radio-optical intraday variables are systematically different objects than the highly variable UV /X-ray –bright sources (Urry 1996).

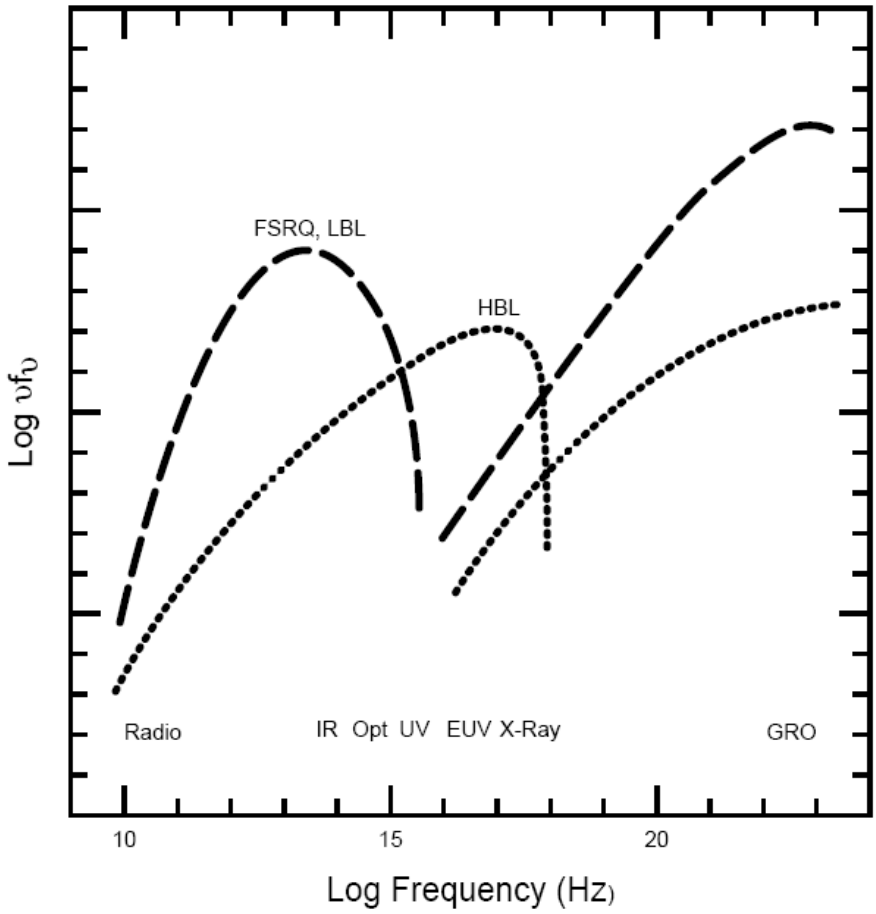

Figure 8: Schematic broad-band spectra of blazars from radio through TeV gamma rays. The low-energy component is probably due to synchrotron radiation and the high-energy component to inverse Compton scattering of lower-energy seed photons, possibly the synchrotron photons or ambient UV /X-ray disk or line photons. Two different curves represent the average spectral shapes (Sambruna et al. 1996) of HBL (dotted line) and LBL (dashed line) as defined by their ratios of X-ray to radio flux. Strong emission-line blazars (FSRQ) have continua like LBL (Sambruna et al. 1996) (*source: Urry* 1996)

2.5 Dependence of the spectrum shape

(See Heuge&Falcke and references therein)

In this section we will look at conditions which influence shape of the blazar spectral continuum. The most interesting for us is the synchrotron component since it defines shape of the spectrum in optical range.

In case of synchrotron radiation, the emitting particles are usually not in thermal equilibrium, but can rather be described with a power-law distribution for a certain range of $\gamma_1 < \gamma < \gamma_2$:

$$N(\gamma)\mathrm{d}\gamma = C\gamma^{-p}\mathrm{d}\gamma \tag{13}$$

The normalization constant C is related to the number (and therefore energy) density of the particles. Adopting typical values of $p = 2$ and $\gamma_2/\gamma_1 \sim 10^4$, we can calculate the expected flux density F_ν measured from a spherical source with radius R at a distance D:

$$F_\nu = \frac{\mathrm{d}W}{\mathrm{d}t\mathrm{d}\nu\mathrm{d}V} \cdot \frac{\frac{4}{3}\pi R^3}{4\pi D^2} \tag{14}$$

which leads to

$$F_\nu \approx 200\mathrm{Jy} \left(\frac{B}{\mathrm{mGauss}}\right)^{3.5} \left(\frac{R}{\mathrm{kpc}}\right)^{3} \left(\frac{\nu}{\mathrm{GHz}}\right)^{-0.5} \left(\frac{D}{\mathrm{Gpc}}\right)^{-2} \tag{15}$$

This is obviously very strongly dependent on the magnetic field strength and the size of the emitting region. So in case we obtain spectral indices, we can calculate the spectral energy distribution F_ν from (4) and therefore estimate B. From spectral indices we can also calculate power-law index p of the electron energy distribution.

3 Variability of blazars

3.1 Introduction

In section 2 we discussed "average" colors of blazars. It means we did not consider changes of colors of particular blazars and for every one of them we considered that we observed its average color index. In this section we will discuss whether this is justified (i.e. the color index changes only little) or not (i.e. color indices change and they change a lot).

3.2 Time scales of the blazar variability

3.2.1 Long-term variation

It was found that the light curves of blazars show variations over time scales of months to years, e.g., 3C 273 (Terrel&Olsen 1972), 3C 446 (Kinman 1975) and 3C 120 (Jurkevich 1971) etc. We call the variations over time scales of years as long-term variation. With the report of periodicity in OJ 287 (Sillanpaa et al. 1988), the OJ-94 project was proposed to detect the expected outburst of OJ 287, which was really observed (Sillanpaa et al. 1996a, b). Some other sources were also found to display long-term variations (Liu et al. 1995; Fan et al. 1997, 2001a, 2002; Fan&Lin 2000a, b; Fan 1999, 2001; Raiteri et al. 2001; Ciprini et al. 2003, 2004). To search for long-term variations, one should have a long time coverage of observations, therefore monitoring programme is important for periodicity analysis.

For the long-term periodicity of variations, there are several explanations, the binary black hole model, the helical jet model, the slim disk model, and the effect of external perturbations to the accretion disk (Sillanpaa et al. 1988, Meyer&Meyer-Hofmeister 1984, Hioruchi&Kato 1990, Abraham&Romero 1999, Fan et al. 1997, 1998a, Villata&Raiteri 1998, 1999, Romero et al. 2000c, 2004, Torrell et al. 2003, Rieger&Mannheim 2000, 2003, Riger 2004). Fan (2005) thinks that this kind of variations in AGNs are associated with the binary black hole systems. And this system was really found by Komossa et al. (2003), who found a binary black hole system in a Seyfert galaxy. However, it should be kept in mind that the present binary black hole system is perhaps too simple. In OJ 287, the optical outburst is not always consistent with radio activity.

Begelman et al. (1980) have considered binary black hole models for active galactic nuclei with orbit periods of the order of 10 yr. They pointed out that the geodetic precession period in a black hole binary system generally exceeds 10^4 yr. Thus it is impossible that the $\sim$ 10 yr period is caused by the precession of a relativistic jet on and off the line of the sight. In the binary black hole model of Sillanpaa et al. (1988), the tidal perturbations of sufficient strength create global disturbances in the disk and cause a flow of

matter into the center of the disk. They consider that two mass points (black holes) are initially in an elliptic orbit. The larger mass point is surrounded by a self-gravitational disk of matter which is tidally perturbed by the smaller mass point. The disk lies in the orbital plane of the binary, and it rotates in the same sense as the binary. Using simulation, one can get the variation pattern and the mass of the smaller black hole can also be estimated by the short time scale, $M \sim 10^6 M_\odot \Delta t(\mathrm{min})$. In this sense, one can estimate mass of the primary black hole. But there is a problem, why is the short time scale caused by the smaller black hole?

If the long-term variation period is caused by a slim disk, then the period can be expressed as (Fan 1999)

$$P = 9.0\delta \left(\frac{\alpha}{0.1}\right)^{-0.62} \left(\frac{M_{\rm BH}}{10^6 M_\odot}\right)^{1.37} \mathrm{yr} \tag{16}$$

But this method gives less massive black hole mass ($\sim 10^7 M_\odot$).

Abraham&Romero (1999) and Romero et al. (2000) proposed a way to explain the long-term period. They assumed that the inner jet and the innermost parts of the accretion disk that surrounds the primary black hole are coupled in such a way that a precession of the disk induces a precession of the jet. A secondary black hole in a close non-coplanar orbit can exert a tidal perturbation on the disk that can result in the near-rigid body precession of its innermost region. But the masses can not be determined uniquely.

For the masses of the central black holes, there are many authors who have tried to determine them (Barth et al. 2002, 2003, Woo&Urry 2003, Bian&Zhao 2004, Cao 2002, Fan et al. 1999, Liang&Liu 2003, Rieger&Mannheim 2000, 2003, 2004, Romero et al. 2000, Wu et al. 2002).

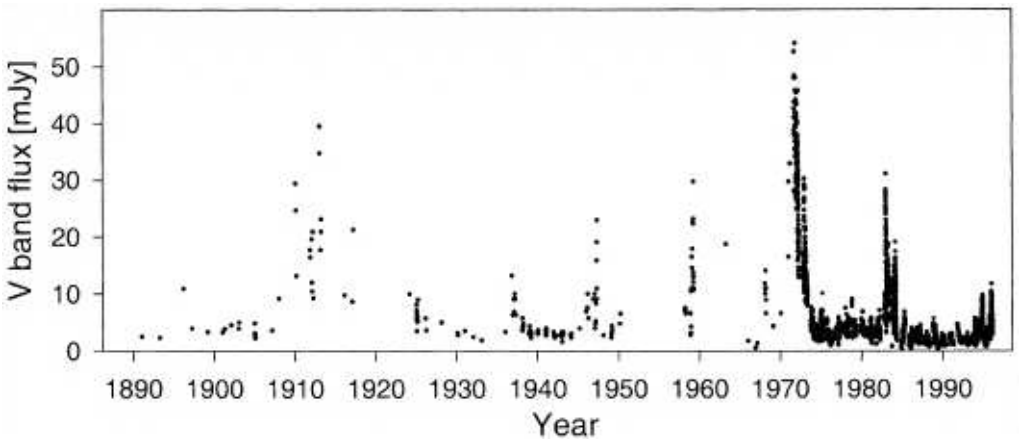

Figure 9: Example of the long-term variability. OJ 287 (*Sillanpaa* 1988)

3.2.2 Short-term variation

Observations also show that the blazars display variations on the timescales of days to weeks and even months, which can be called as short-term variation. In the OJ-94 project, 3C 66A was selected as a comparison source for OJ 287 because it is relative quiescent blazar. However, it was in a bright state during the monitoring programme and displayed a 65day period in its light curve (Lainela et al. 1999). Similar timescale variation was noticed from Mkn 501 which displayed a 23 day variation period in the X-ray and TeV gamma-ray bands (Kranich et al. 1999). It may be possibly related to the orbital motion of the relativistic jet emerging from the less massive black hole (Fan 2005). Due to the orbital motion around the center of mass, the Doppler factor for the emission region is a periodical function of time (Rieger&Mannheim 2000, 2003, Rieger 2004). For 3C 66A, its 65-day period implies that a shock wave (see section Shock-in-jet models) moves along a helical path in a relativistic jet. Therefore the shocks can explain why the periodicity can be detected during the bright state but not in the faint state of the 3C 66A (Lainela et al. 1999).

3.2.3 Intraday variation

During the past decades, the evidence for the existence of variability on scale of days has been established for blazars. These night to night variations are called intraday variations. Such as 1.2 mag variation from AO 0235+164 during a week long observation period (Romero et al. 2000), but they found no spectral index variation when the source showed large variation during their observational period. However, Raiteri et al. (2001) found a flattening spectral index when the source brightened.

Intraday variation can give an upper limit to the mass of the central black hole if the time scale indicates the innermost stable orbit period. The inner most stable orbit depends on the black hole and the accretion disk.

$$r = \frac{6GM}{c^2} \tag{17}$$

for thin accretion disks surrounding a Schwarzschild black hole,

$$r = \frac{4GM}{c^2} \tag{18}$$

for thick accretion disks surrounding a Schwarzschild black hole, and the radius of the event horizon of a Kerr black hole of mass M and an angular momentum parameter a,

$$r = 1.48 \times 10^5 \left(1 + \sqrt{1 - a^2}\right) \frac{M}{M_\odot} \tag{19}$$

The period is

$$P = \frac{2\pi r}{c} \tag{20}$$

The mass can be obtained from the period determined from the light curves.

Considered as a simple causality argument, the intraday variability time scale perhaps sheds some light on the size of the emitting region since the variability cannot be faster than the light-crossing time of the emitting volume. Thus the observed variability time scale gives an upper limit to the size,

$$R \leq c\Delta t_{\rm var} \tag{21}$$

or

$$R \leq c\delta\Delta t_{\rm var} \tag{22}$$

if the emitting volume moves at relativistic velocity (all equations Fan 2005).

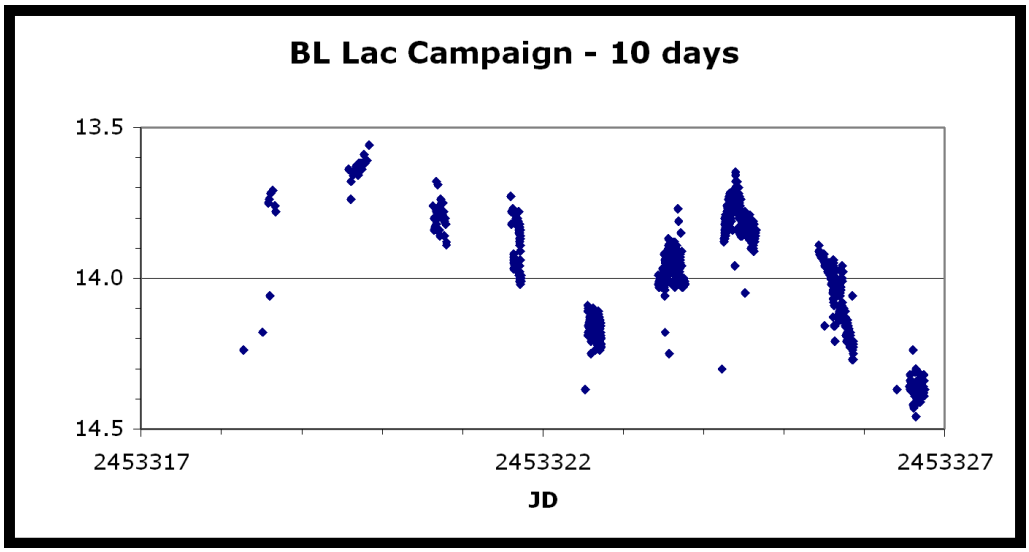

Figure 10: Example of the intraday variability. BL Lacertae. Nov. 2004 (*AAVSO*)

3.2.4 Microvariability

Variations on scale of minutes or hours are called microvariations. Recently, some sources were reported to show these variations. Such as 0.5 mag variations in both R and V bands within a single night from AO 0235+164 (Romero et al. 2000). Very rapid brightness increasing by 1.3 magnitudes over 2.0 hours in optical region was found from 0736+017 by Clements et al. (2003). A rapid variation of 0.3 mag over 3 hours was also observed from BL Lacertae in observation done in Oct. 2000 in Georgia (Fan et al. 2004). In the OJ-94 monitoring programme, very dense light curves displayed continuous variability on time scales from minutes to days (Takalo et al. 1999; Tosti et al. 1999; Pursimo et al. 2000).

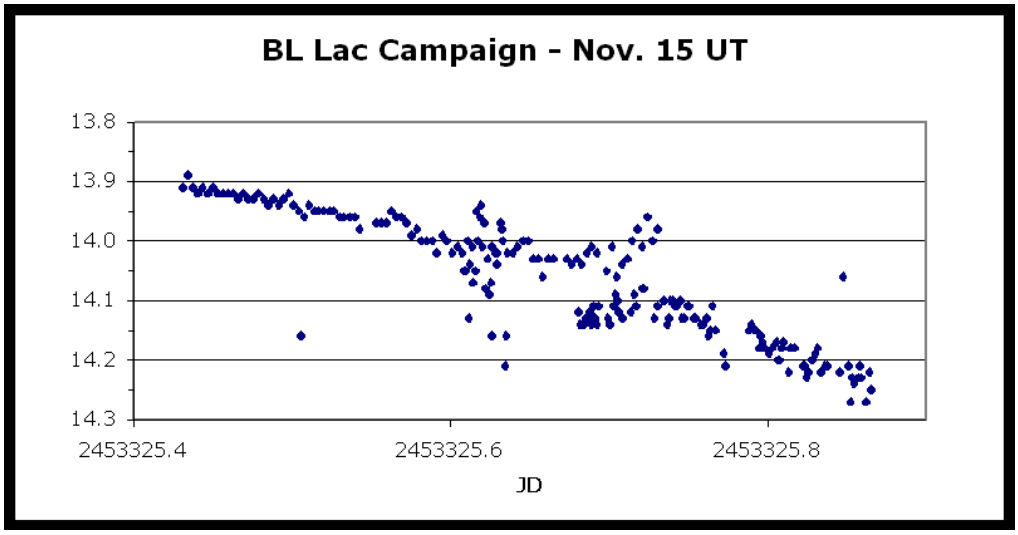

Figure 11: Example of the microvariability. BL Lacertae. (*AAVSO*)

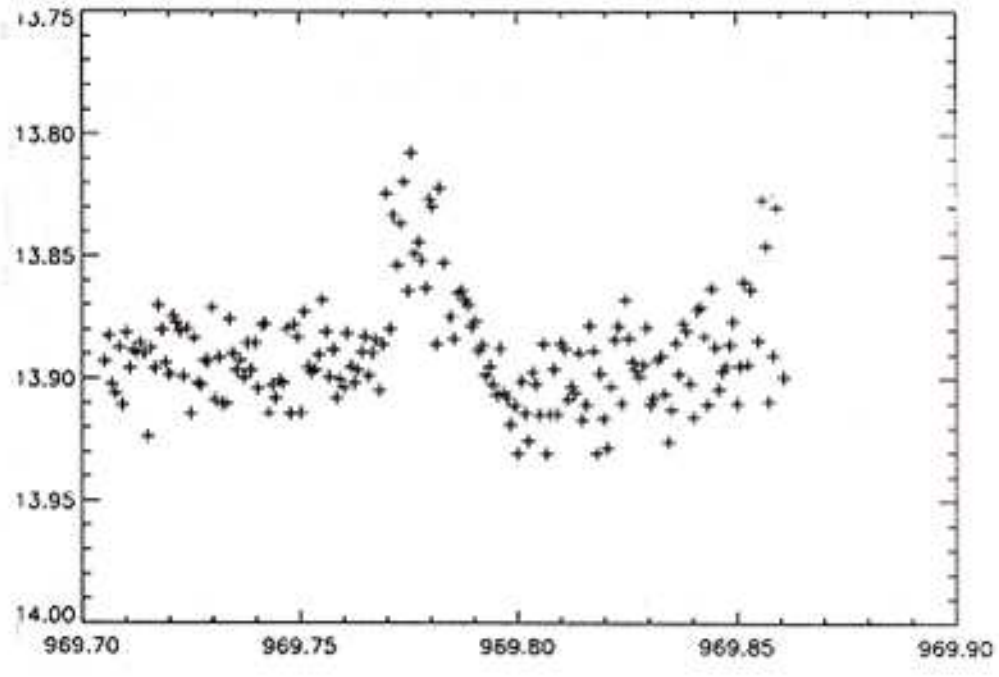

Figure 12: Another example of the microvariability. Mrk 501. (*Carini* 1982)

3.3 Causes of the blazar variability

Variability in blazars can be caused by several effects. It can be either intrinsic or extrinsic causes. To extrinsic causes belongs microlensing and interstellar scintillation and to intrinsic causes belong processes inside the active galaxy and the jet such as geometric effects, shocks in the jet and processes in the accretion disk. We will look at these effects more closely.

3.3.1 Interstellar scintillation

Interstellar scintillation (ISS) is an intensity variation observed as a result of the wavefronts from a distant radio source being perturbed by refractive index fluctuations in the turbulent, ionized interstellar medium (ISM) of our Galaxy. ISS are observed only in the most compact radio sources, such as pulsars and flat-spectrum AGN.

Over the last decade or so, evidence has accumulated to demonstrate that scintillation is the principal cause of the rapid, radio intra-day variability (IDV) observed at frequencies of several GHz in some quasars and BL Lac objects (Bignall et al. 2004).

Observations of ISS, interpreted in the light of theoretical models, constrain properties of both the Galactic ISM turbulence, and the scintillating sources themselves; namely angular size and structure on microarcsecond scales, smaller than even VLBI can reach! Thus ISS studies can contribute to our knowledge of the inner radio jets in distant AGN.

I will not pursue this effect any deeper because as it was said, it affects only radio wavelengths and not the optical region, which we are interested in.

3.3.2 Microlensing

A gravitational lens is formed when the light from a very distant, bright source is "bent" around a massive object (such as a massive galaxy) between the source object and the observer. The process is known as gravitational lensing, and was one of the predictions made by Einstein's general relativity. Chang&Refsdal (1979) suggested that gravitational lensing of distant quasars would not only be caused by the deflection of light by the potential of intervening galaxies, but may also be caused by the fine-scale structure of the potential well, i.e. from individual stars within galaxies that are sufficiently close to the line of sight.

In a gravitational lens, the gravity from the massive object bends light like a lens. As a result, the path of the light from the source is curved, distorting its image, and the apparent location of the source may be different from its actual position. In addition, the observer may see multiple images of a single

source. If the source, massive object, and the observer lie on a straight line, the source will appear as a ring behind the massive object.

Microlensing is a class of the gravitational lensing, where no distortion in shape can be seen but the amount of light received from a background object can be changed. Image deflection is small and images fall on top of each other resulting in one magnified image. If the lens (or source) is in motion relative to the source (or lens) or observer moves, AND image resolution is below angular separation, we see amplitude or brightness variations. What to expect from these changes?

- Symmetric Outburst
- Frequency independence of outburst across spectrum
- Duration of outburst is related to lens speed
- Microlensing predicts correlated, simultaneous outbursts in widely separated frequency bands

The typical angular fluctuation associated with a microlensing event caused by a lens at distance D (at $z \ll 1$) is (Paczynski 1986)

$$\Delta\theta \sim 4.5 \left(\frac{M}{M_\odot}\right)^{1/2} \left(\frac{D}{100\mathrm{Mpc}}\right)^{-1/2} \mu\mathrm{arcsec}. \tag{23}$$

The characteristic timescale for the event is given by the time required for the lens to move transversely by a distance equal to the typical impact parameter (Paczynski 1986)

$$\Delta t \sim 4 \left(\frac{M}{M_\odot}\right)^{1/2} \left(\frac{D}{100\mathrm{Mpc}}\right)^{1/2} \left(\frac{v}{500\mathrm{km/s}}\right)^{-1} \mathrm{yr}. \tag{24}$$

Webb et al. (2000) found evidence for a microlensing event in the 1997 outburst of AO 0235+164. Outburst exhibited a double-peaked morphology, and durations, amplitudes and morphologies are similar in each frequency band. They concluded that AO 0235+164 is a great candidate for a microlensing with "line-of-sight" intervening galaxy and that 1997 outburst is consistent with microlensing.

However, there are also facts opposing the microlensing. For example Kayser (1988) concluded that intense optical outbursts are unlikely to be due to microlensing. Primary objection is timescales for radio and optical events. Foreseeable blazar models should allow us to determine if actual lensing properties, masses, velocities, are realistic.

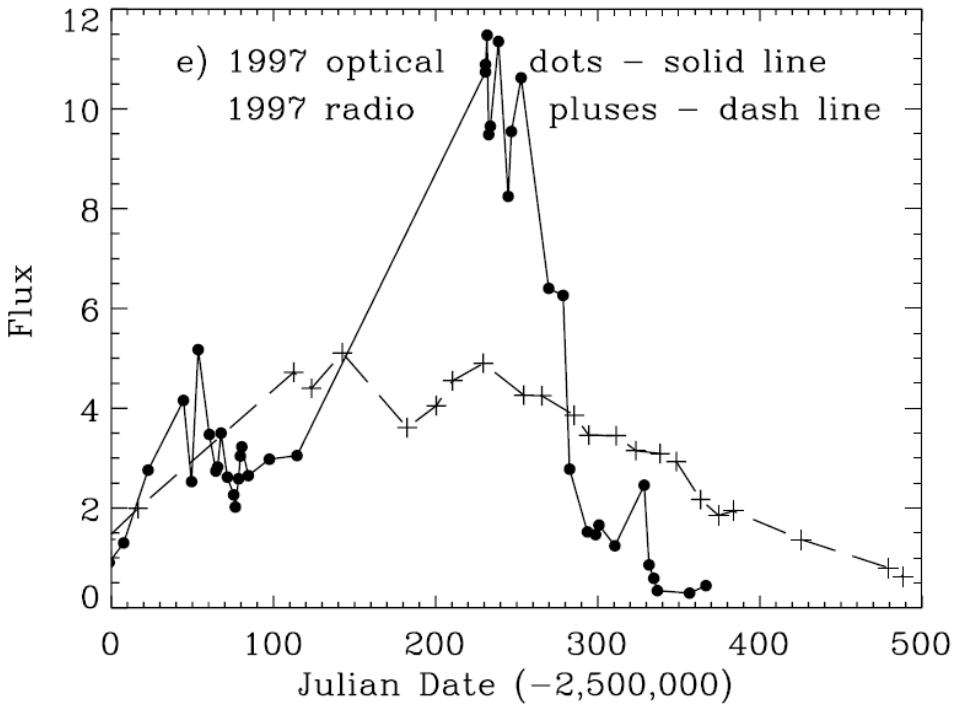

Figure 13: The 1997 outburst of AO 0235+164. The close correlation between the second radio peak and the optical peak remains the strongest evidence for microlensing during the outburst. (*Webb et al.* 2000)

3.3.3 Accretion disk models

The formation of highly relativistic jets in active galactic nuclei is one of the most fundamental open problems in astrophysics. Two main classes of models for the formation of jets consider either extraction of rotational energy from a rapidly spinning black hole (Blandford&Znajek 1977) or magnetohydrodynamic winds arising from the inner regions of accretion disks (Blandford&Payne 1982). In both scenarios the magnetic field must play a major role in channeling power from the black hole or from the disk to the jet. In both cases, it should be sustained by matter accreting onto the black hole, leading to expect a relation between the accretion power and the jet power (Maraschi&Tavecchio 2003). The flaring states observed in blazars could be a consequence of the way in which the jet is fed with energy, mass, and angular momentum from the accretion disk. A flare could occur when a significant amount of energy has been accumulated in the inner disk and is subsequently expelled into the jet (Donea&Biermann 2002).

Observations of rapid X-ray variability in Seyfert galaxies (Lawrence &Papadakis 1993), and intraday optical variability in radio quiet QSOs (Sagar et

al. 1996) are explicable in terms of bright spots on accretion disks (Abramowicz et al. 1991, Mangalam&Wiita 1993). The key idea of these models is that any intrinsic variability produced in or just above an accretion disk will be strongly modulated by the orbital motion of the radiating flare. Both Doppler effects and purely general relativistic light bending effects come into play, and are particularly important for fluctuations produced in the inner portions of accretion disks. Phenomenological bright spot models were first applied to X-ray time series and were shown to produce excellent fits to generic light curves and their power spectral densities (Abramowicz et al. 1991). They were also shown to be viable models for the smaller optical fluctuations in blazars and other AGN (Mangalam&Wiita 1993).

Although various physical causes for such fluctuations have been considered, none has been worked out to the extent to provide fully convincing pictures. Vortices forming within a disk (Abramowicz et al. 1992) could be relevant, as could plasma dominated events just above the disk surface (Krishan&Wiita 1994). Spiral shocks produced in the accretion disk around a black hole by passing massive stars, molecular clouds or companion black holes could also yield suitable luminosity fluctuations from the disks (Chakrabarti&Wiita 1993). The possibility that self-organized criticality plays a role in producing many flares of different strengths has also been seriously considered (Mineshige et al. 1994, Wiita&Xiong 1997).

3.3.4 Geometrical effects

It is important to understand the accidental (geometric) modulations to separate them from physical mechanisms. Geometrical effects may introduce variations or alter amplitudes, time scales, and flares considerably. Among most accepted geometrical effects belongs binary black hole model, helical jet model, jet swinging etc.

Binary black hole system presents an opportunity that, due to the gravitation of the second black hole, the whole system with the jet may undergo precession on time scales consistent with observed changes in light curves of blazars. Doppler factor is angle dependent and so, due to relativistic beaming, even a small change in the direction of the jet caused by the precession could be the source of brightness changes. However, it does not have to be only the precession of the system, which changes direction of the jet, but the second black hole may cause gravitational lensing if orbiting near the jet.

Helical jet models assume knots or blobs of plasma spiraling in the jet. Camendzin&Krockenberger (1992) contend that knots of enhanced particle density are injected at a finite jet radius. There, every volume element of plasma has finite angular momentum and moves on a helical trajectory due to the superposition of the outflow and a circular motion. In knots moving relativistically on helical trajectories, the direction of forward beaming varies

with time. For an observer close to the jet axis the beam sweeps across the line of sight, introducing flares due to the lighthouse effect as in pulsars (Wagner&Witzel 1995). This will lead to quasi-periodic variations of a few oscillations, and may cause complex light curves if the contributions of several knots are superposed. VLBI observations of curved trajectories of individual knots, sometimes accompanied by changes in angular velocity, are interpreted as an indication that the plasma is indeed moving on 3D helical trajectories. Schramm et al. (1993) and Wagner et al. (1995) used these models to explain long-term variations of 3C 345 and PKS 0420-014. It is unclear whether the quasi-periodic oscillations of IDV can also be explained by this model. In particular, it is unclear whether the assumed constant acceleration can be provided.

3.3.5 Shock-in-jet models

(This whole section is based solely upon private communication with prof. Alan Marscher, founder of this model.)

Major increase in either the bulk velocity or internal energy of the jet flow will cause shock waves to form and propagate down the jet. The function of shock waves is to decelerate supersonic flows to subsonic speeds. Hence, a forward shock decelerates the downstream fluid that it overtakes such that, in the rest frame of the shock front, the fluid velocity becomes subsonic downstream of the shock front. The shock front therefore propagates supersonically relative to the downstream fluid. A reverse shock, on the other hand, slows high-velocity upstream fluid entering the shocked region from behind down to subsonic speeds, as measured in the frame of the reverse shock front. The reverse shock front propagates downstream, but more slowly than does either the forward shock front or the upstream, unshocked gas. A given disturbance can have only a forward shock or both a forward and a reverse shock, with the relative strengths of the shocks depending on the details of the time-variable flow.

A shock front compresses the plasma (which causes an increase in the density as well as an increase in the internal energy) and enhances the component of the magnetic field that lies parallel to the shock front, both by the inverse of a factor called the compression ratio. The shock may additionally accelerate relativistic particles. The acceleration is most efficient when the magnetic field lies perpendicular to the shock front, since the required particle streaming occurs most freely along the field lines. Hence, amplification of the synchrotron emission in shocks results from

- the increase in density behind the shock front
- the increase in the magnetic field strength and adiabatic heating of the electrons for fields parallel to the shock front

- diffusive shock acceleration of the electrons for fields perpendicular to the shock fronts

If the shock accelerates particles only at the shock front, then the highest energy electrons will suffer radiative losses such that they only maintain these high energies over a short distance. The highest frequency radiation can therefore be emitted only within a thin sheet behind the shock front. The thickness of this sheet increases as the frequency decreases until the frequency is so low that radiative losses are neglible across the entire shocked region. This frequency stratification of the emission in a shock provides a duality that explains very nicely the general characteristics of the multiwaveband light curves of blazars: a flare caused by a shock is spread across many decades of frequency, yet the timescale of variability can be much shorter at higher frequencies, owing to the thinness of the emission region behind the shock front that results from radiative energy losses of the electrons.

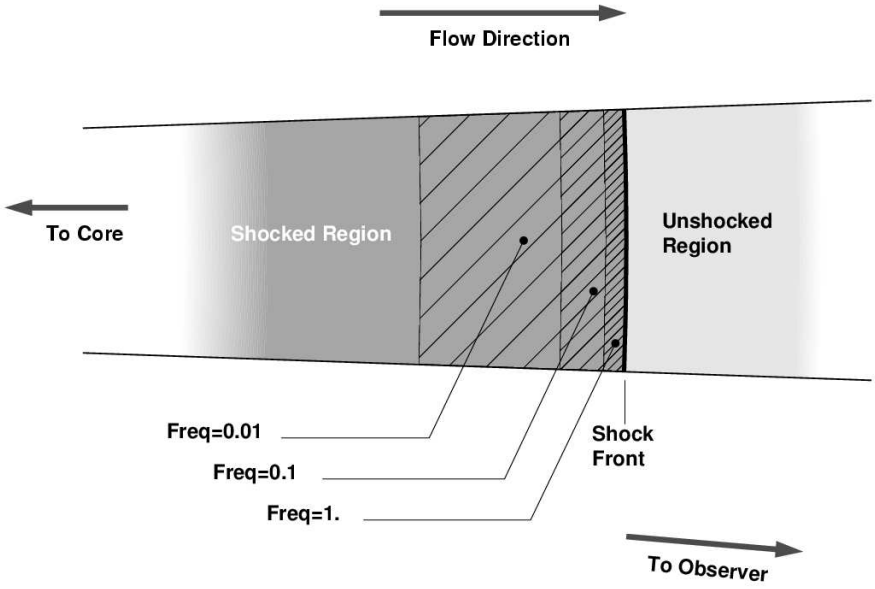

Figure 14: Sketch of a shock in a relativistic jet, with arbitrary scaling. The hatched regions show the sites of emission at different frequencies. The frequencies are scaled such that a value of 1.0 is at the high-frequency end of the synchrotron or inverse Compton spectrum. (*Marscher&Travis* 1991)

The general evolution of a shock-induced flare in a jet is as follows.

1. The Compton stage, in which the electron energy loss is dominated by synchrotron self-Compton scattering. The flux density rises while the self-absorption turnover changes only slightly, perhaps even decreasing with time. The multiwaveband νF_ν spectrum should show the γ-ray portion containing the bulk of the non-thermal apparent luminosity.

Not all shocks will go through this phase - it probably requires extreme conditions.

2. The synchrotron stage, in which the energy loss is mainly from synchrotron radiation. The flare spectrum propagates to lower frequency with the peak flux density (at the self absorption turnover) changing slowly or not at all. It is possible that this "sideways" spectral evolution is the main factor responsible for the flat overall spectrum of a typical blazar below the turnover frequency.

3. The adiabatic stage, in which the flare declines as the shock expands down the jet. This phase is also described by Hughes et al. (1985), who show how shocks can explain variations in radio polarization.

The γ-ray and X-ray flux in a shock-induced flare should therefore peak first, followed by the optical and infrared and then radio, as described above.

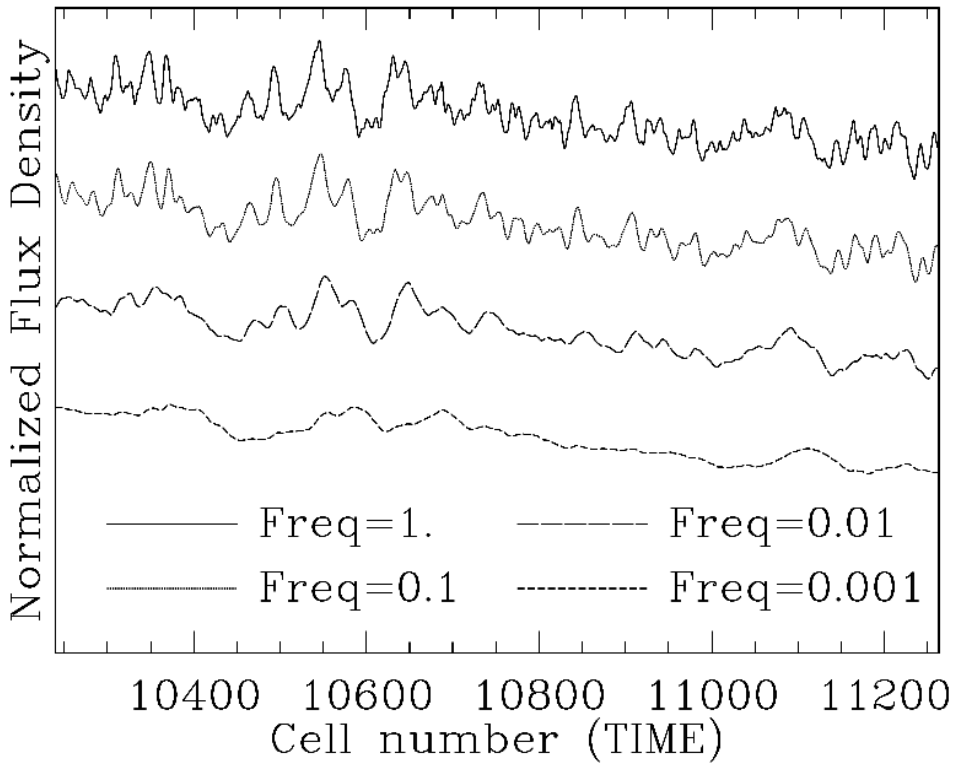

Figure 15: Flickering in the light curve of a blazar as a shock propagates down a hydromagnetically turbulent jet. The frequencies are scaled such that a value of 1.0 is at the high-frequency end of the synchrotron or inverse Compton spectrum. The slow decline of the flux density is caused by the evolution of the overall emission from the shock, while the rapid variations result from turbulent cells passing into and out of the emission region at that given frequency. (*Marscher&Travis* 1991)

4 Analysis of data

4.1 Introduction

Blazars represent physically extremely important case of Active Galactic Nuclei, AGN. They exhibit violent activity and variability over a very wide range of energy and time. They are luminous high-energy sources. Through investigation of blazars, various processes of generation of high energy photons can be studied and analyzed.

As important, luminous, and variable high energy astrophysical sources, the blazars represent one of significant working fields for the Group of the high Energy Astrophysics in the Stellar department of Astronomical Institute of the Academy of Sciences of the Czech Republic in Ondřejov. In this study, we focus on novel approach of studies of these objects: color and spectral analyses of selected blazars, in analogy to color analyses of Optical Afterglows of Gamma Ray Bursts performed by this group which proved to deliver valuable additional scientific information to understand the physical processes in the source as well as the source environment. This represents, in our opinion, the novel approach to the investigations of blazars and AGNs in general, with resulting in interesting consequences.

The spectral energy distribution (SED) of BL Lacs from the radio to the X-ray range is dominated by non-thermal emission due to synchrotron radiation. FSRQs show also strong emission lines and a thermal contribution that may be comparable to the synchrotron emission in the optical spectral region. The study of SED properties is an excellent diagnostic tool for theoretical models. There is a handful of very interesting information related to the physical properties of the emitting region. However, as far as variability is concerned, many emission models are still unable to reproduce and predict the variability features observed in every region of the spectra. A kind of simplification is obtained by considering time evolution in a selected region of the spectra, for example in the optical. The optical region is very narrow with respect to other spectral regions, nevertheless it may yield a large amount of information if there is a large dataset to analyze. In this case, the complication is the possible presence of other components in addition to the synchrotron continuum. For example, thermal emission from the accretion disk around the central engine, the emission from the surrounding regions of the nucleus, the host galaxy contribution. The purpose of this analysis is to list and analyze the main features of the optical SED for an extended sample of blazars, primarily composed of BL Lac Objects.

We report on $UBVR_{\rm c}I_{\rm c}$ Johnson-Cousins bands observations of 33 blazars obtained from several blazar catalogues (Xie 1994, Xie 1999, Raiteri 1998, Guibin 1995, Guibin 1998, Fiorucci 1996, Villata 1997, Villata 2000, Bai 1998, Bai 1999, Belokon 1999). From a statistical analysis of the optical

spectral continuum we derive information on the characteristics of this class of objects, and constrain theoretical models.

4.2 Characteristics of the dataset

Table 1 reports the object list, sorted by increasing right ascension. Column 1 reports the IAU name, Columns 2-5 give the source designation, the coordinates and the redshift as indicated by Simbad (http://simbad.u-strasbg.fr). The photometric data were corrected for galactic interstellar reddening using the extinction values listed in the Nasa Extragalactic Database (http://nedwww.ipac.caltech.edu). Column 6 contains values of the reddening in V band. The last column in Table 1 is devoted to a first classification of blazars (see Section 2.4). This tentative classification is an attempt to clarify the enigmatic nature of these sources, but the distribution among these sub-types is ambiguous, as several sources show intermediate behavior. The numbers are obtained from the catalog of Donato et al. (2001). Authors did the classification of blazars mainly from values of radio to X-ray spectral indices.

Our dataset contains 11 LBLs, 19 HBLs, and 2 FSRQs (or sources which have strong thermal contributions at optical wavelengths). It is easy to verify that our sample of blazars is biased toward the BL Lac Objects. This is partially due to the fact that photometric broad-band analysis is easier for this class of sources, thanks to the relative absence of lines in their spectrum.

4.3 The optical spectral flux distribution

The optical flux densities (expressed in mJy) were obtained from dereddened standard magnitudes using the calibration of Vega (Harmanec, private communication):

$$mag_{\rm blazar} - mag_{\rm Vega} = -2.5 \log \left(\frac{F_{\rm blazar}}{F_{\rm Vega}} \right) \tag{25}$$

with conversion factors reported by Bessell (1979). From the same author we have adopted the effective wavelengths corresponding to the $UBVR_{\rm c}I_{\rm c}$ broad bands, neglecting the changes due to the different spectra of the observed sources.

With the data we have analyzed the presence of a power law $f(\nu) \sim \nu^{-\alpha}$ searching for linear fits on a $\log \nu - \log(\nu f(\nu))$ scale. The assumption is that the dereddened spectral flux distribution in the optical range can be described by a single power law (see Figs. 16, 17). We have accepted only the data that allow us to calculate the regression based on at least three

Table 1: List of the selected blazars. Columns 2-5 contain names and information as reported by Simbad (http://simbad.u-strasbg.fr). Column 6 gives an interstellar coefficient obtained from Nasa Extragalactic Database (http://nedwww.ipac.caltech.edu). The last column contains the blazar class.

IAU name (B1950)	Common name	Coordinates (J2000) α	δ	z	$A_{\rm v}$	Class
0109+224	S2 0109+22	01 12 05.8	+22 44 39	0.40+	0.124	LBL
0145+138	B 0145+138	01 48 29.8	+14 02 19	0.125	0.194	HBL
0219+428	3C 66A	02 22 39.6	+43 02 08	0.444	0.279	LBL
0235+164	AO 0235+164	02 38 38.9	+16 37 00	0.940	0.265	LBL
0317+185	2E 0317+183	03 19 51.3	+18 45 35	0.190	0.458	HBL
0323+022	2E 0323+0214	03 26 13.9	+02 25 14	0.147	0.372	HBL
0347-121	B 0347-121	03 49 23.2	-11 59 57	0.188	0.156	HBL
0414+009	2E 0414+0057	04 16 52.4	+01 05 24	0.287	0.393	HBL
0420-014	B 0420-014	04 23 15.8	-01 20 33	0.915	0.436	FSRQ
0422+004	PKS 0422+00	04 24 46.8	+00 36 07	0.310	0.335	LBL
0502+675	1ES 0502+675	05 07 56.3	+67 37 24	0.314	0.504	HBL
0548-322	PKS 0548-322	05 50 40.6	-32 16 16	0.069	0.117	HBL
0735+178	PKS 0735+17	07 38 07.4	+17 42 19	0.645	0.116	LBL
0737+746	B 0737+746	07 43 59.6	+74 33 50	0.315	0.091	HBL
0754+100	PKS 0754+100	07 57 06.7	+09 56 35	0.280	0.075	LBL
0818-128	OJ -131	08 20 57.4	-12 58 59		0.197	
0829+046	PKS 0829+046	08 31 48.9	+04 29 39	0.180	0.108	LBL
0851+202	OJ 287	08 54 48.9	+20 06 31	0.306	0.094	LBL
0912+297	B2 0912+29	09 15 52.4	+29 33 24		0.081	HBL
1028+511	B 1028+511	10 31 18.5	+50 53 35	0.360	0.041	HBL
1118+424	1ES 1118+424	11 20 48.0	+42 12 12	0.124	0.059	HBL
1133+704	Mrk 180	11 36 26.4	+70 09 27	0.046	0.044	HBL
1147+245	OM 280	11 50 19.2	+24 17 54	0.200	0.090	LBL
1215+303	ON 325	12 17 52.1	+30 07 01	0.130	0.079	HBL
1424+240	PKS 1424+240	14 27 00.5	+23 48 00	0.160	0.194	HBL
1517+656	H 1517+656	15 17 47.6	+65 25 23	0.702	0.084	HBL
1641+399	3C 345	16 42 58.8	+39 48 37	0.594	0.044	FSRQ
1652+398	Mrk 501	16 53 52.2	+39 45 36	0.033	0.064	HBL
1727+502	I Zw 187	17 28 18.6	+50 13 11	0.055	0.098	HBL
1749+096	OT 081	17 51 32.8	+09 39 01	0.322	0.598	LBL
1959+650	B 1959+650	19 59 59.9	+65 08 55	0.048	0.587	HBL
2154-304	H 2154-304	21 58 52.1	-30 13 32	0.117	0.071	HBL
2254+074	PKS 2254+074	22 57 17.3	+07 43 12	0.190	0.219	LBL

quasi-simultaneous ($\Delta t < 2$ h) photometric bands. It is worth noting that in most blazars we observe spectral hardening with increasing flux. This is fully consistent with most theoretical models (see Section 3.3) where this is often called a "bluer-when-brighter" tendency.

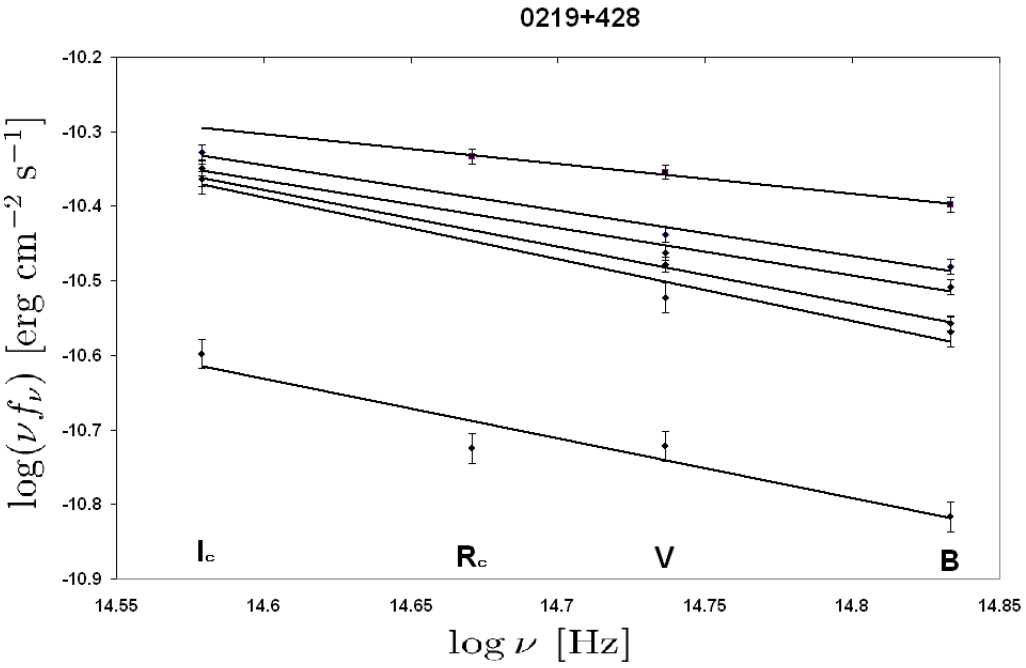

Figure 16: The spectral power distribution of 0219+428 in the optical region with a selection of different continuum spectra. A weak flattening with increasing flux is visible.

4.4 Discussion

The dereddened spectral flux distribution in the optical wavelengths can be analyzed alone, considering the time evolution, and/or compared with the time-averaged multiwavelength SED. What we expect to see depends on the type of blazar, because this information (i.e. the blazar type) tells us where the synchrotron emission is peaked.

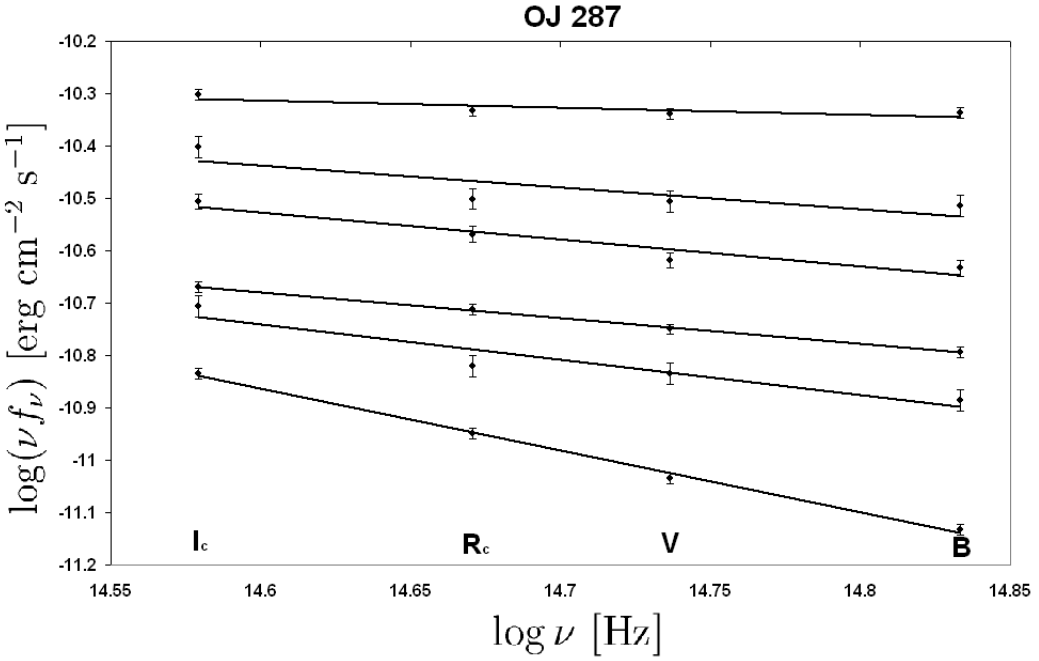

Figure 17: The spectral power distribution of OJ 287 (0851+202) in the optical region with a selection of different continuum spectra.

4.4.1 LBLs

Optical observations play an important role in discriminating between LBLs and HBLs. In the first case, we expect to be in the descending part of the spectral power distribution, after the maximum, while in the latter case the maximum is located at higher frequencies and we are in the ascending part (See Figs. 8, 18). Thus we expect an average spectral index $\alpha > 1$ for LBLs, and $\alpha \leq 1$ for HBLs. The histograms in Fig.19 show that this result is confirmed for the LBLs, where the slope is always > 1. As a result, in our sample α clusters around 1.5. For a partially cooled electron distribution, in the power-law form $N(E) = N_0 E^{-p}$, and with an isotropic pitch angle distribution, the standard emissivity for the synchrotron total spectrum is

$$J_{\rm syn}(\nu) \sim N_0 B^{(1+p)/2} \nu^{(1-p)/2} \tag{26}$$

This implies that

$$\alpha = \frac{p-1}{2} \tag{27}$$

We have shown for LBLs that α is near 1.5, which corresponds to $p \sim 4$.

In the case of radiative losses dominated by Synchrotron Self-Compton (SSC) emission, the time-averaged synchrotron spectrum becomes:

$$J_{\rm syn}(\nu) \sim \nu^{(1-p)/2-(4-p)/2} \tag{28}$$

Because of the near-constant shape of the particle distribution, the synchrotron emission above the break energy will have a roughly constant time-averaged spectral shape $F_\nu \sim \nu^{-1.5}$. Moreover, Chiang&Bottcher (2002) demonstrated that for a broad range of particle injection distributions, synchrotron self-Compton(SSC)-loss dominated synchrotron emission exhibits exactly this kind of spectral slope (i.e. $\alpha \simeq 1.5$). From this point of view, SSC models fit very well the optical emission for LBLs, while for the HBLs we have to consider X-ray observations if we want an accurate fit.

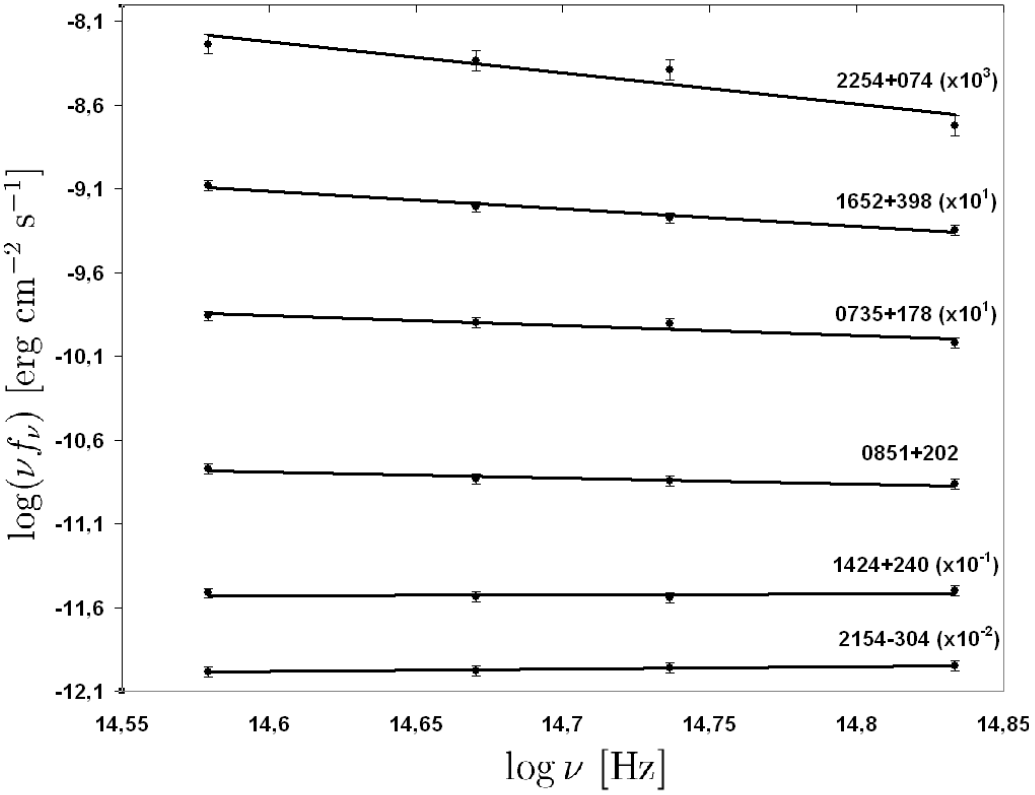

Figure 18: Examples of optical spectral power distributions obtained with our data. Sources are ordered according to their average value of α. Note that the fluxes have been opportunely scaled to have a progressive order.

4.4.2 HBLs

The fact that LBLs show an average spectral slope steeper than HBLs was expected. However, the histogram of the two classes partially overlap. The HBL spectral slope scatters in the range between 0.8 and 2.2, while we expected $\alpha \leq 1$ (though the peak really is between 0.8 and 1.0). Therefore a classification based on the optical spectral slopes would not correspond exactly to the one adopted in Table 1. Thus the optical emission of some HBLs

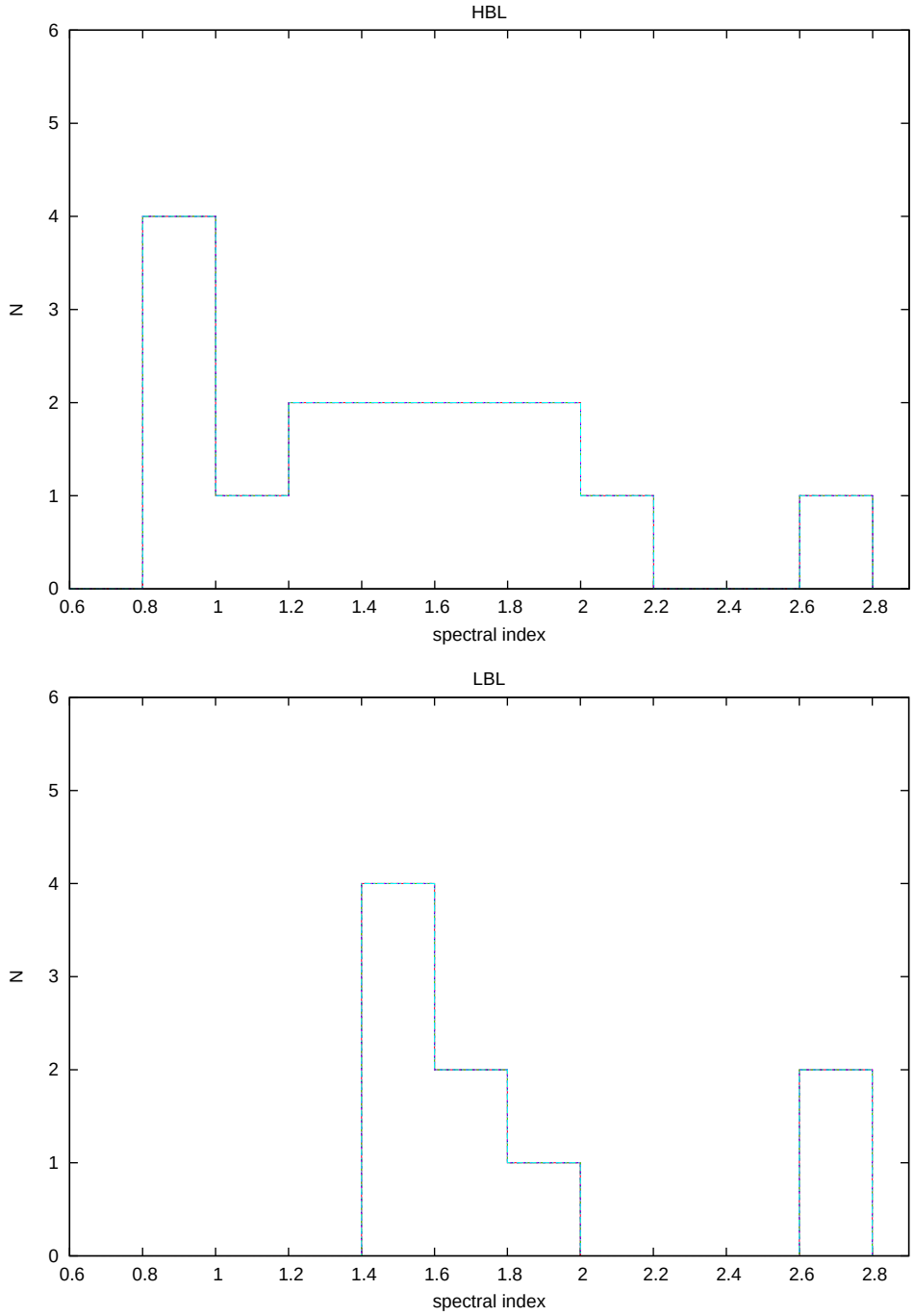

Figure 19: Histogram of the mean spectral index for the HBLs (top) and LBLs (bottom).

is contaminated by other components. In conclusion, the fact that the optical spectral slope of HBLs can be anywhere in range shown in the histogram can be the sign of a SED deformation around the optical region for some of these blazars. Such a deformation may be due to a thermal contribution to the overall optical signal, or to non-thermal emission coming from different regions of the jet with respect to those that dominate the SED at higher frequencies.

From the range of $\alpha = 0.8-2.2$ we get from the Eq. 27 $p = 2.6-5.4$. However, if we consider Eq. 28 and the numerical simulations of Chiang&Bottcher (2002) we see that spectral index α is not so sensitive to p in a wide range of p.

4.4.3 FSRQs

The situation is similar for the FSRQs, since their optical emission is strongly contaminated by thermal emission from the accretion disk and the surrounding regions. Of particular relevance is the presence of the so called "blue bump" which flattens the spectral slope in the optical region. Although our statistics are very poor for this type of blazars, both FSRQs in our sample show strong variability, a fact that is generally attributed to the synchrotron emission.

4.4.4 Spectral slope variability

From our set of photometric measurements in three or four bands, we are able to investigate possible relations between the source luminosity and the slope of the optical spectral energy distribution. The level of correlation sheds light on the non-thermal emitting processes involving synchrotron and inverse Compton cooling of the electron population in the active region.

Figure 20 shows the instantaneous spectral slope α as a function of the $R_{\rm c}$ flux density (as done in Massaro&Trévese 1996). The plot represents only a subset of the data, but it may be considered representative of the overall set. Strong scattering (which is only partially explainable with statistical fluctuations) is evident. The more variable blazars also show a general slope-flattening trend when the source is brighter (see bluer-when-brighter tendency above).

This phenomenon is quite common in blazars. It may be explained in different ways. For example, it may be the sign of the presence of two components that contribute to the overall emission in the optical region, one variable and the other stable. It is also possible to explain it with a one-component synchrotron model: the more intense the energy release, the higher the particle's energy.

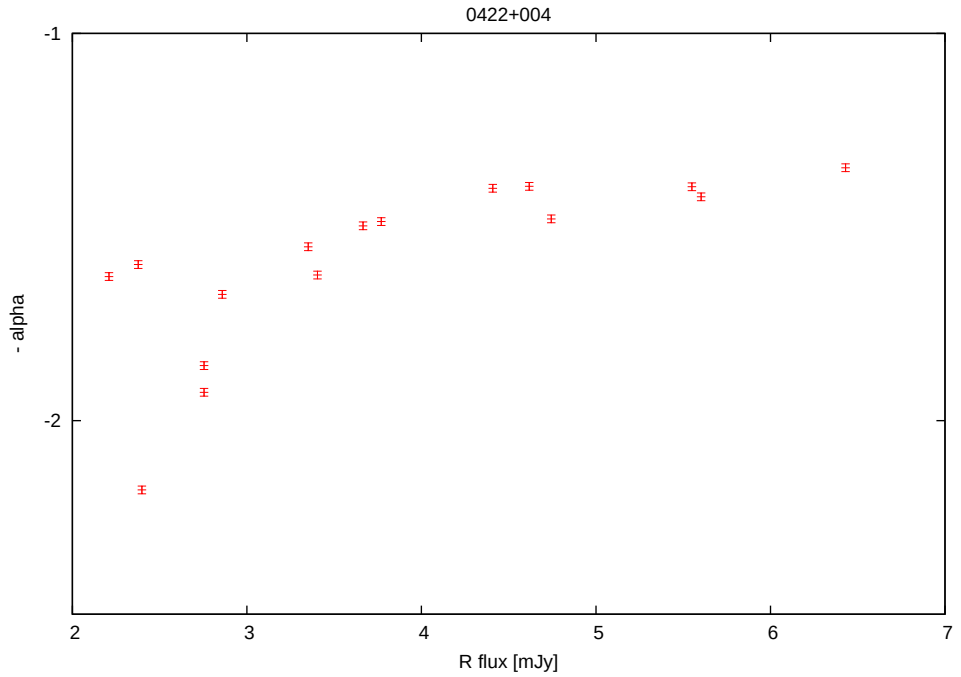
0422+004
-1
-2
- alpha
2
3
4
5
6
7
R flux [mJy]

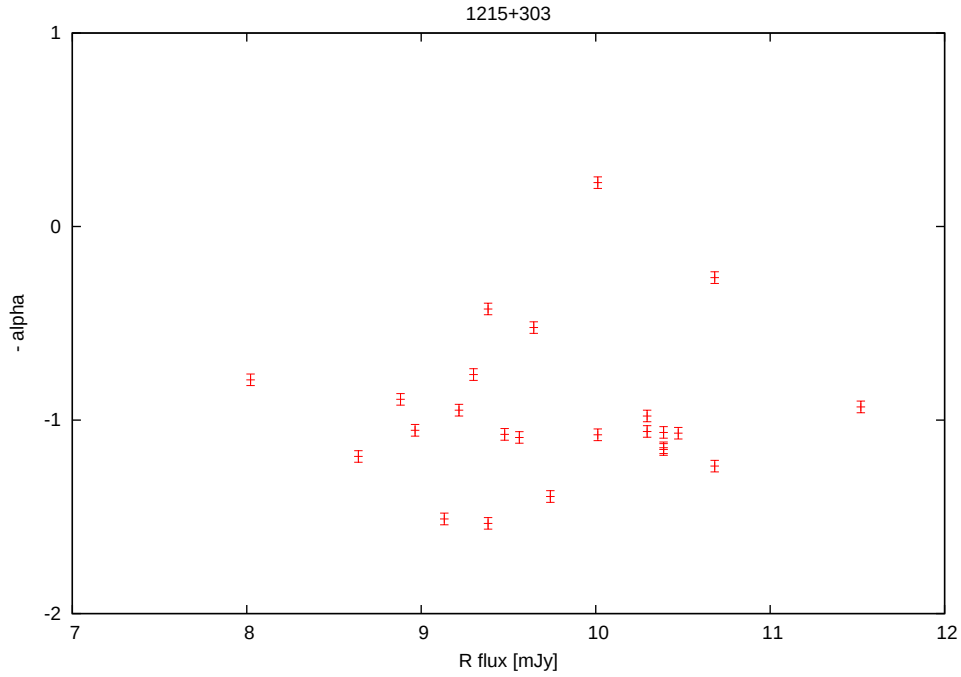
1215+303
1
0
-1
-2
- alpha
7
8
9
10
11
12
R flux [mJy]

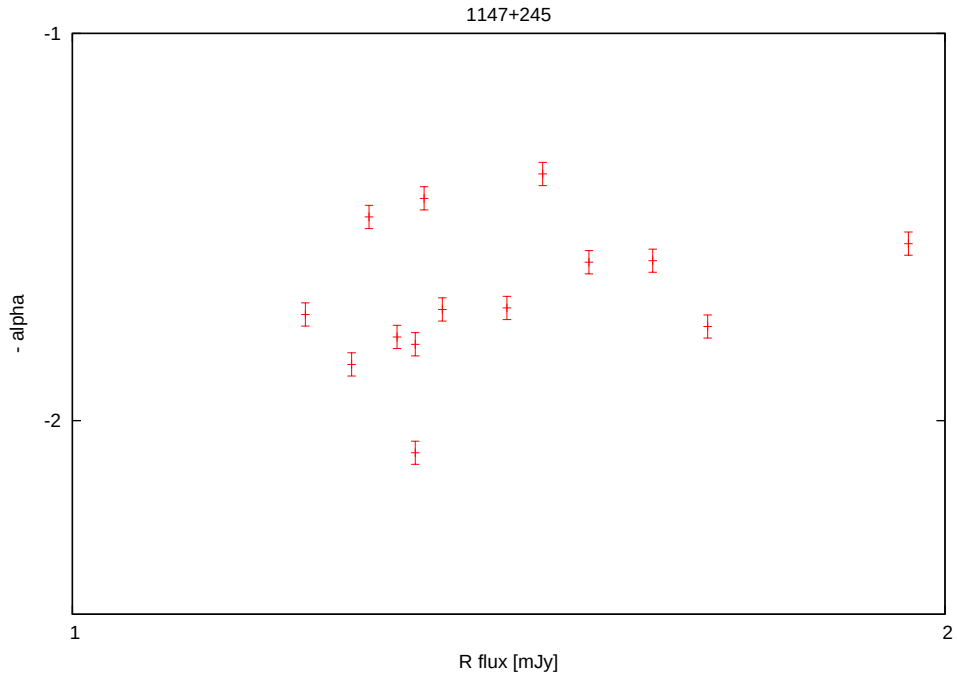
1147+245
-1
-2
- alpha
1
2
R flux [mJy]

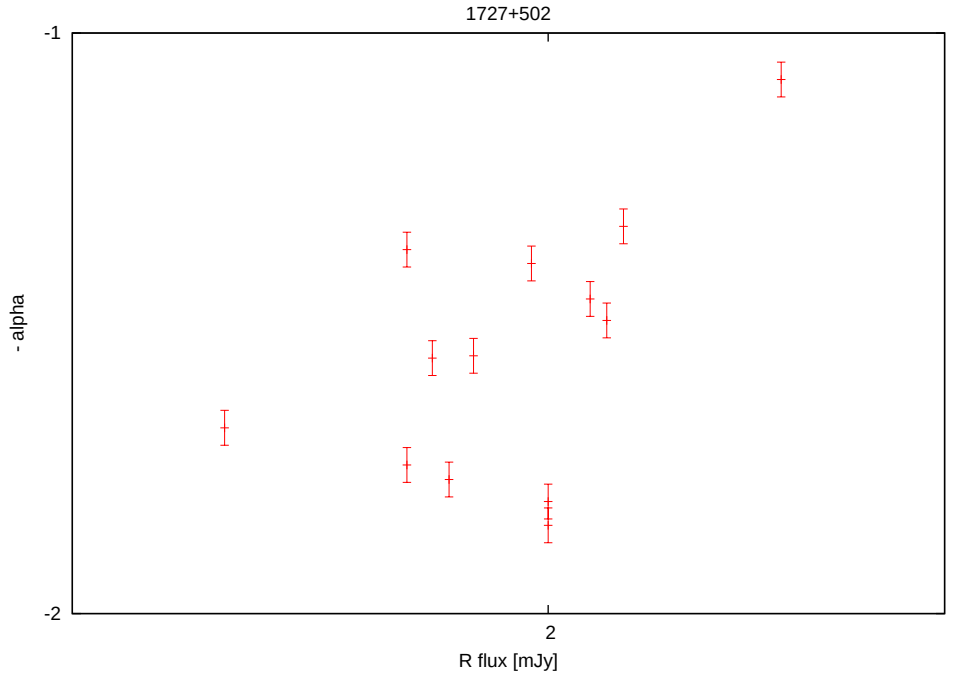
1727+502
-1
-2
- alpha
2
R flux [mJy]

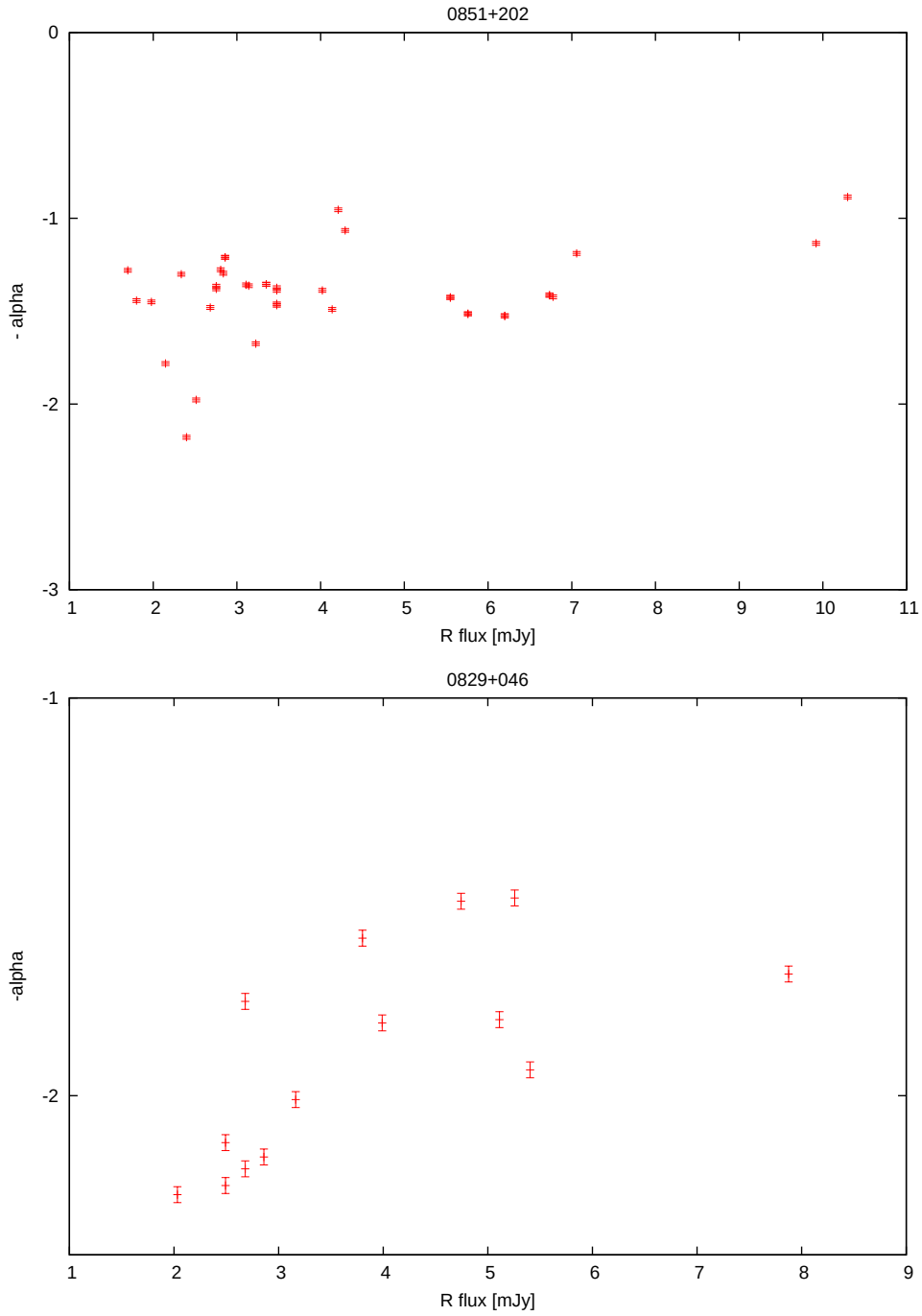

Figure 20: Dependence of the spectral slope on intensity for a subset of blazars. The scattering, which is only partially explainable as statistical fluctuations, is evident. The more variable blazars show a general trend that flattens the slope when the source is brighter.

4.5 Color analysis of blazar sample

The study of color properties of blazars has been initiated by promising and physically important results provided for another class of extragalactic sources, namely Optical Afterglows of GRBs which results are briefly summarized and discussed below (for more details see Šimon et al. 2001 and 2003).

Color indices have been and still are widely used in the study of many phenomena in astrophysics. Even quite recently the use of broad-band colors has been advocated for identification of young type Ib/c SN (Gal-Yam et al. 2004). For the study of optical afterglows (OAs) of GRBs this powerful method is only very rarely applied, therefore in this field it is still quite innovative. Color indices enable us to resolve small variations of the profile of the spectra of the OAs from the measurements in the commonly used $UBVRI$ filters. This method proved to be very useful for the analysis of the common properties of the OAs (Šimon et al. 2001). It also allows us to constrain the properties of the local interstellar medium of GRBs inside their host galaxies.

The color indices of the optical afterglows (OAs) of the gamma-ray bursts (GRB) are a powerful tool to use in the search for the common properties of these events. The OAs in the fireball model represent the stadium when the matter from the central engine, moving at the relativistic speed, interacts with the surrounding interstellar medium by means of external shocks. The color indices of the OAs can be used as an important parameter reflecting the related physical processes. Besides the astrophysical analysis, the specific color indices of OAs give hope to resolving whether an optical transient event is related to a GRB even without available gamma-ray detection. Most afterglows appear to concentrate in the well localized regions of $V-R$ vs. $R-I$ and $B-V$ vs. $V-R$ diagrams. Colors of all OAs analyzed here correspond to their final decline branch with the exception of the first point of $GRB970508$. The color indices

$(R-I)_0 = 0.46 \pm 0.18$

$(V-R)_0 = 0.40 \pm 0.13$

$(B-V)_0 = 0.47 \pm 0.17$

appear to be typical (Šimon et al. 2001). OAs therefore appear quite red in the spectral region between the I and B filter (colors similar to mid-G or early K stars). On the other hand, the $(U-B)_0$ index of the OAs is negative with a large scatter and the position of the afterglows in (U-B) vs. (B-V) diagram is often quite different from other sources. These specific colors can be used to distinguish genuine OAs related to GRBs from another types of objects in optical GRB searches. The results reported by Šimon et al. (2001, 2003) are thus extremely significant from the point of view of optical searches for gamma-ray bursters. First, the well defined color of

OAs allows, together with the power law decline, to distinguish the real OAs of GRBs from the other types of astrophysical objects. So far, only the rapid fading behavior has served to distinguish the genuine afterglows. So we have another tool now, enabling one to analyze images taken in various optical passbands quickly for possible optical counterparts of GRBs, without waiting for the following night to confirm the rapid object fading. Secondly, the well focused position of OAs in color-color diagrams represents a very important tool to consider independent (on satellite projects) optical searches for OAs of GRBs. Although there are suitable databases available for this kind of analyses such as the deep UKSTU archival plates, the search for real OAs was difficult because of high background level of other types of variable phenomena not related to GRBs. The combination of fading profile with the color information may be used as a very powerful tool to search for real OAs in suitable databases with color information such as the UKSTU archive. It should be noted that the actual rate of OAs may exceed those of GRBs due to different beaming in gamma-rays and in optical (Hudec 2000). Moreover, the OAs detected by optical searches may provide very precise localizations of GRBs, and hence allow detailed studies of their host galaxies. On the other hand, the OAs rates and/or limits provided by these analyses could provide constraints on the time and/or wavelength dependent beaming in GRBs, and hence contribute to the understanding of the physical model of the events. The results discussed here also confirm the importance of color information in the strategy of the optical afterglow searches and analyses. Not only the fading profile, but also the color information may yield a valuable physical conclusion regarding the model, the origin, and the position of GRBs. It is important to provide further optical observations of OAs in a well organized way. If possible, the observations should be carried out with standard filters, and various passbands should be taken immediately i.e. during the same night. The strong concentration of the color indices in the color-color diagrams of OAs of GRBs suggests that the intrinsic reddening (i.e. in their host galaxies) must be quite similar for all OAs and, moreover, that this reddening is likely to be rather small. The reason is that in the case of a large reddening it would be quite unlikely to obtain such similar values of absorption in all cases. Notice that there is no apparent scatter of the color indices of the OAs (except for GRB000131) along the reddening path. The scatter in the $U-B$ vs. $B-V$ diagram is large but only in the $U-B$ direction which is inconsistent with the interstellar reddening. All these lines of evidence therefore imply that most GRBs whose afterglows are analyzed here are unlikely to come directly from the inner (densest) parts of the star-forming regions. However, that does not exclude the possibility that these GRBs originate on "our side" of a structured star-forming region. Alternatively, the density and the dust abundance of the local interstellar medium might be substantially reduced by the intense high-energy radiation

of the GRB trigger, as modeled by Waxman&Draine (2000).

We have performed analogous study for blazars in this work. As already stated above, the method of color indices provides powerful tool to investigate both physical processes in the source as well as environment of the source.

We will deal with the colors of blazars, particularly with the fact whether their color indices occur in a wide range of values or not. By this analysis we can find out whether

1. the physical source of emission of blazars (jet, synchrotron radiation - electron energy distribution, magnetic field, etc.) is similar for all of blazars or not. As we have shown in previous chapters, the spectral indices of blazars (corresponding in fact to colors of blazars) support the synchrotron emission from relativistic jets, with electron energy distribution slope being similar for all of blazars.

2. the close environment of blazars as well as light absorption (apart from the Galactic extinction) along the line of sight to the observer is similar for all of blazars or not. In Figs. 21 and 22 we show $(\text{V-R})_0$ vs. $(\text{B-V})_0$ and $(\text{R-I})_0$ vs. $(\text{V-R})_0$ diagrams. We see that the colors of blazars corrected for the Galactic extinction exhibit small scatter in values $(\text{V-R})_0$, $(\text{B-V})_0$ and $(\text{R-I})_0$. Specifically the values of range

   $(B-V)_0 \in (0.00; 1.21)$

   $(V-R)_0 \in (0.18; 0.64)$

   $(R-I)_0 \in (0.38; 0.65)$

   Mean values are:

   $(B-V)_0 = 0.46 \pm 0.22$

   $(V-R)_0 = 0.37 \pm 0.22$

   $(R-I)_0 = 0.55 \pm 0.17$

   All these results imply that even the environment in blazars is likely to be very similar. We see no apparent reddening, which implies that there is no dust along the line of sight or it was destructed by X-rays from blazars.

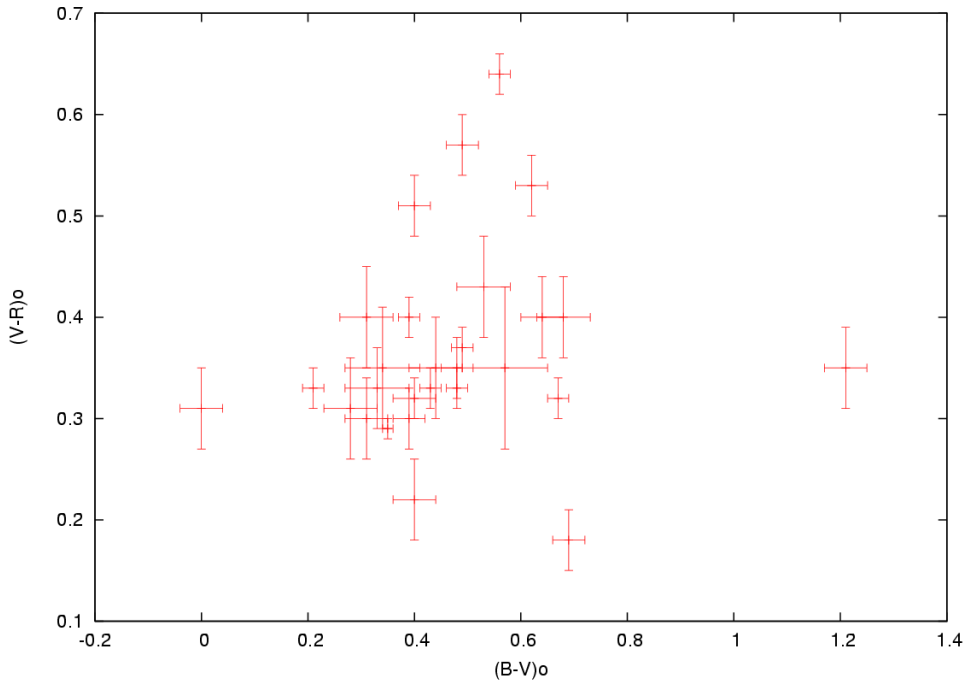

Figure 21: $(V\text{-}R)_0$ vs. $(B\text{-}V)_0$ diagram of blazars

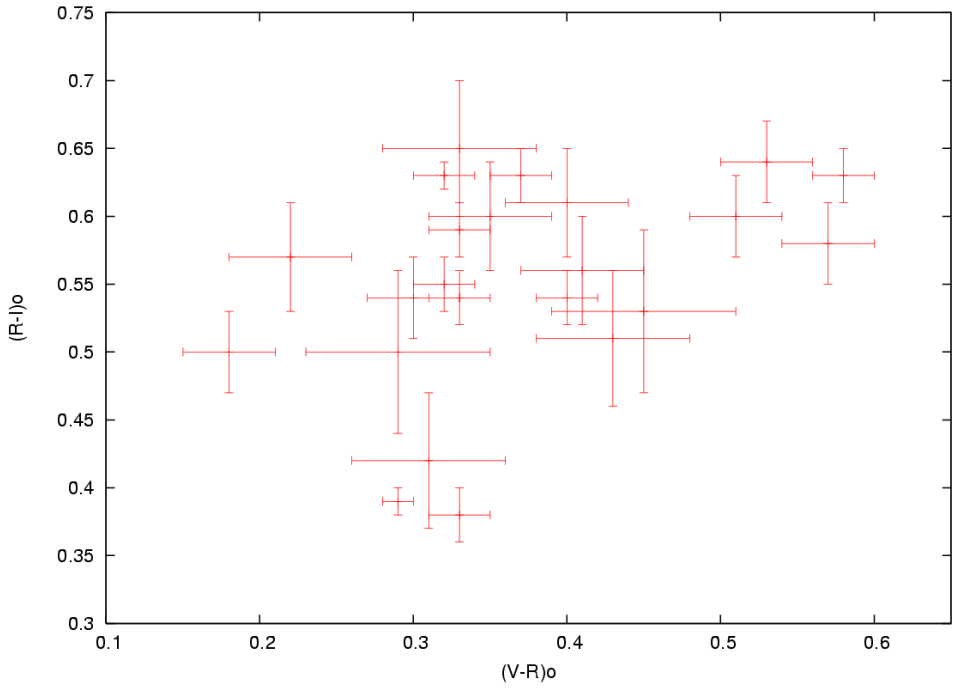

Figure 22: $(R\text{-}I)_0$ vs. $(V\text{-}R)_0$ diagram of blazars

3. colors of blazars can be used for an identification of blazars in sky surveys. If we compare color diagrams of blazars with color-color diagrams of OA of GRB (see Fig. 24 and Fig. 25), we see how alike these objects are in color behavior. On the other hand, compared with general AGN, where the jet is either missing or directed out of Earth, for the AGN we see a scatter in color indices (caused e.g. by reddening) (see Fig. 26 and Fig. 27). If we look at the color indices of the main sequence stars, we see a large differences among values for different spectral types of stars (see Fig. 23). Knowing this wee see that we may use color indices as a tool to distinguish blazars from stars, supernovae and non-active galaxies in sky surveys. Unfortunately, in this way we cannot easily distinguish blazars from AGN and OA of GRB (see Figs. 28 and 29). However, we can select candidates for blazars which can be confirmed or rejected by other criteria (variability, spectrum, polarization, etc.)

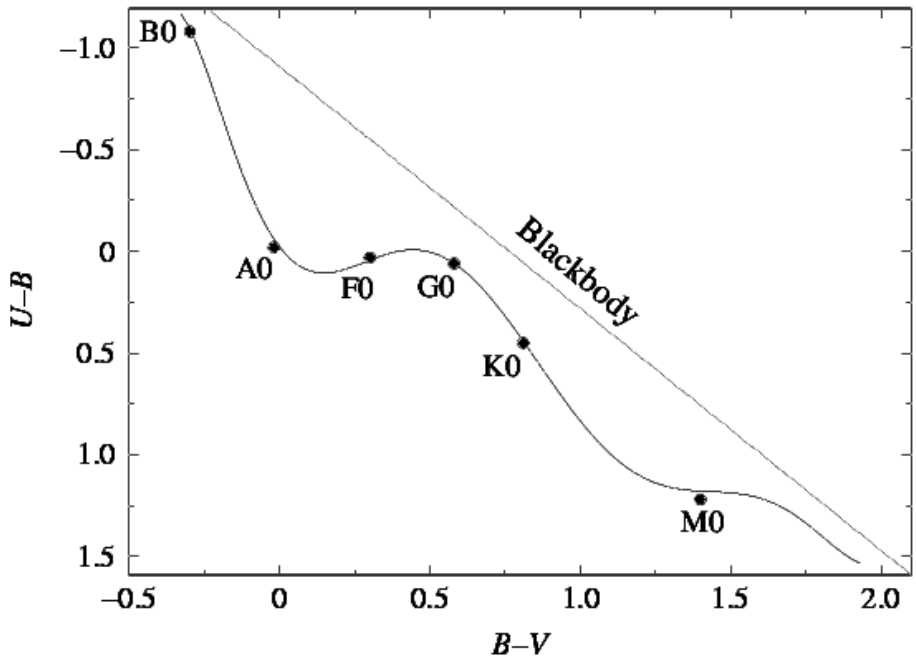

Figure 23: Positions of stars in color-color diagram. (*http://burro.astr.cwru.edu/Academics/Astr221/Light/colors.html*)

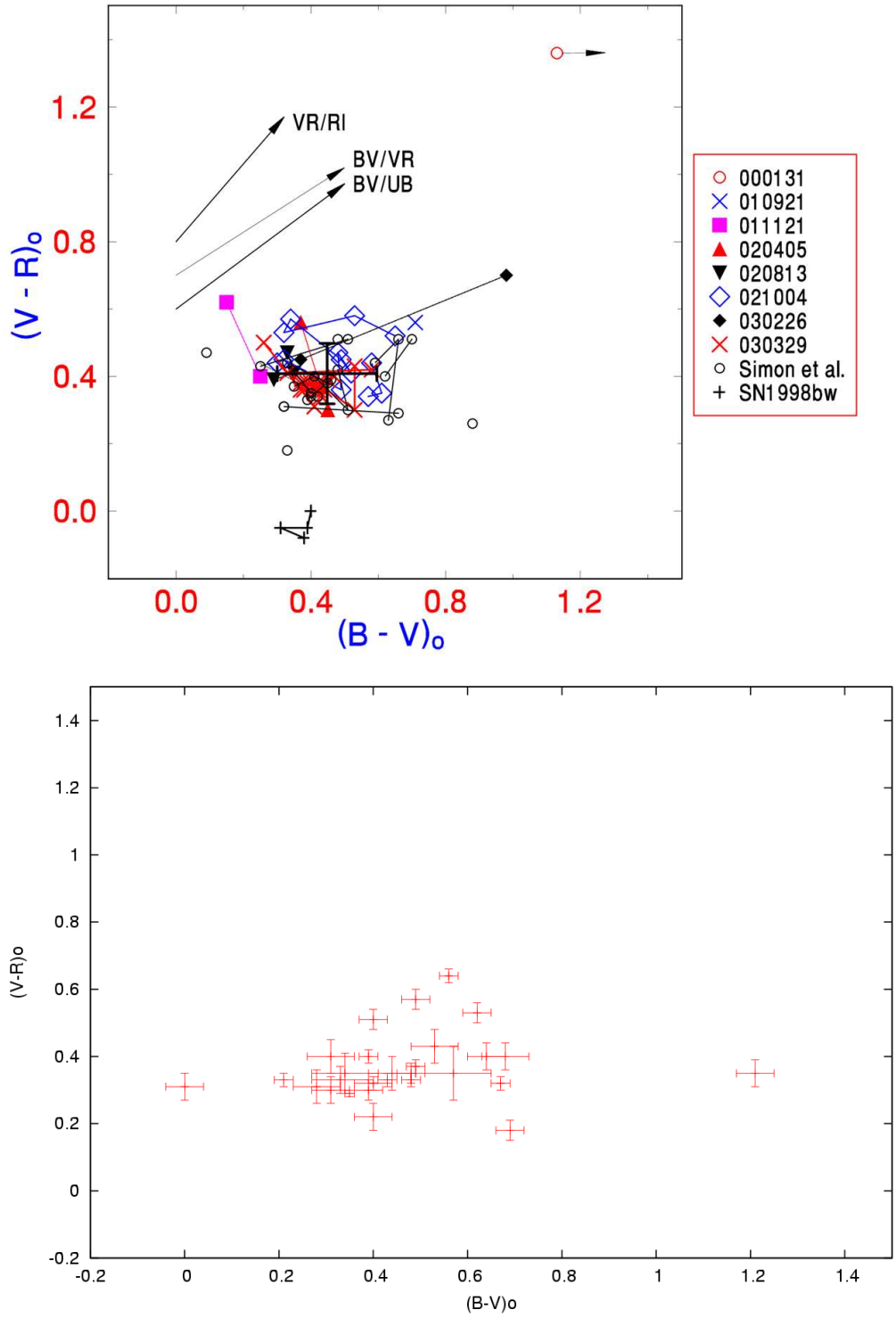

Figure 24: Comparison of $(V\text{-}R)_0$ vs. $(B\text{-}V)_0$ diagrams of GRB and blazars on a same scale. (*GRB data: Šimon et al.* 2001)

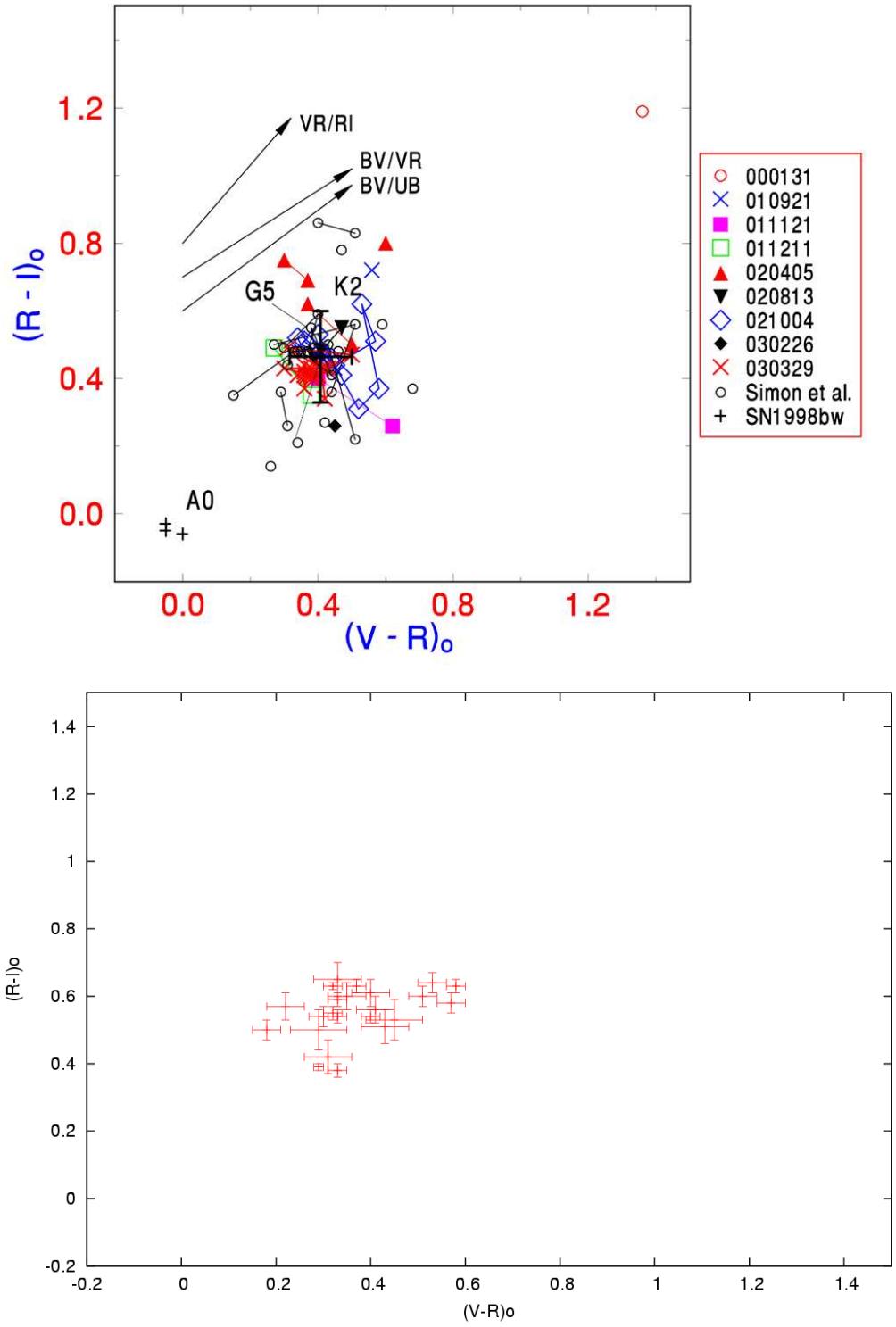

Figure 25: Comparison of $(R\text{-}I)_0$ vs. $(V\text{-}R)_0$ diagrams of GRB and blazars on a same scale. (*GRB data: Šimon et al.* 2001)

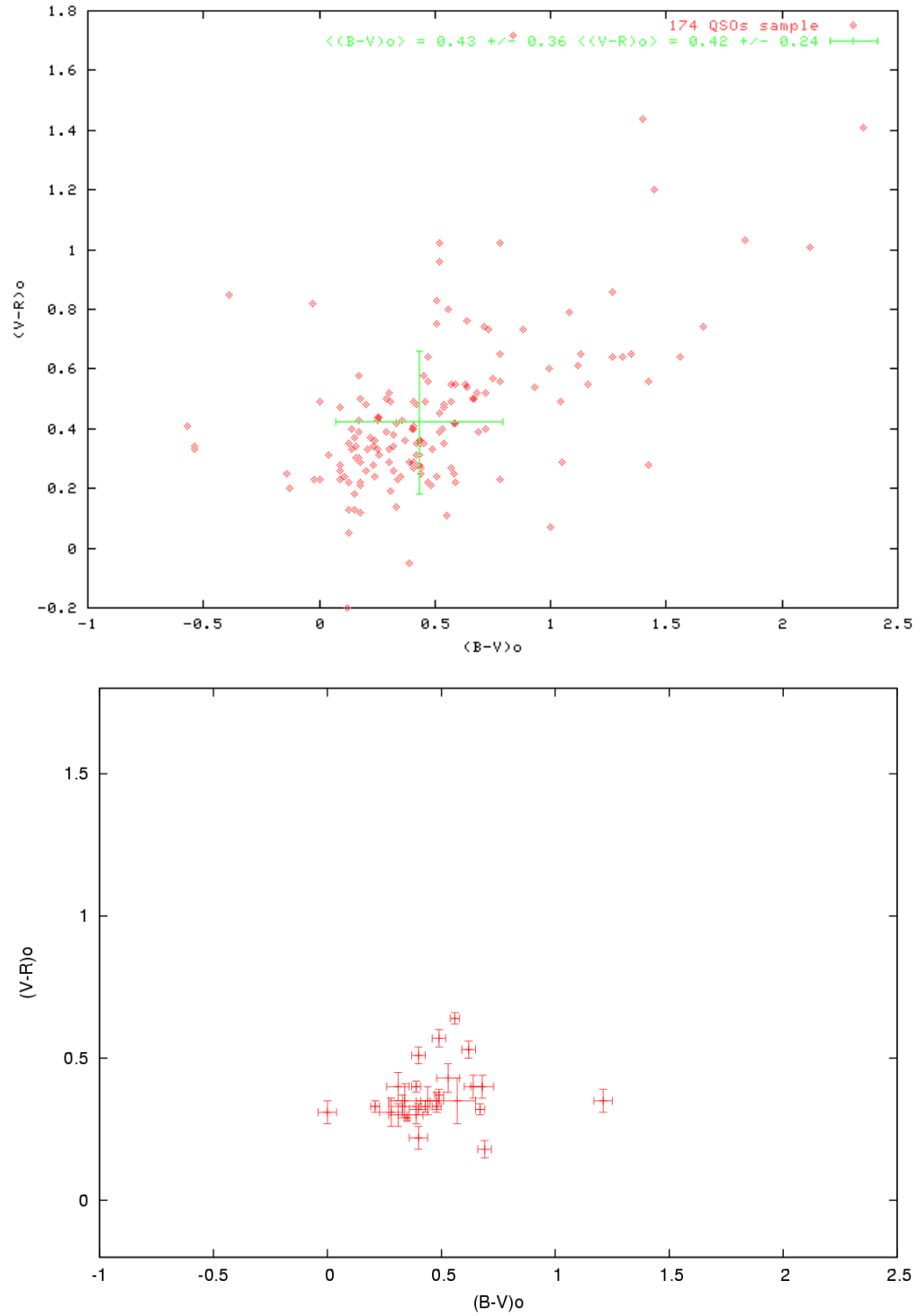

Figure 26: Comparison of $(V\text{-}R)_0$ vs. $(B\text{-}V)_0$ diagrams of AGN and blazars on a same scale. (*AGN data: Topinka* 2002)

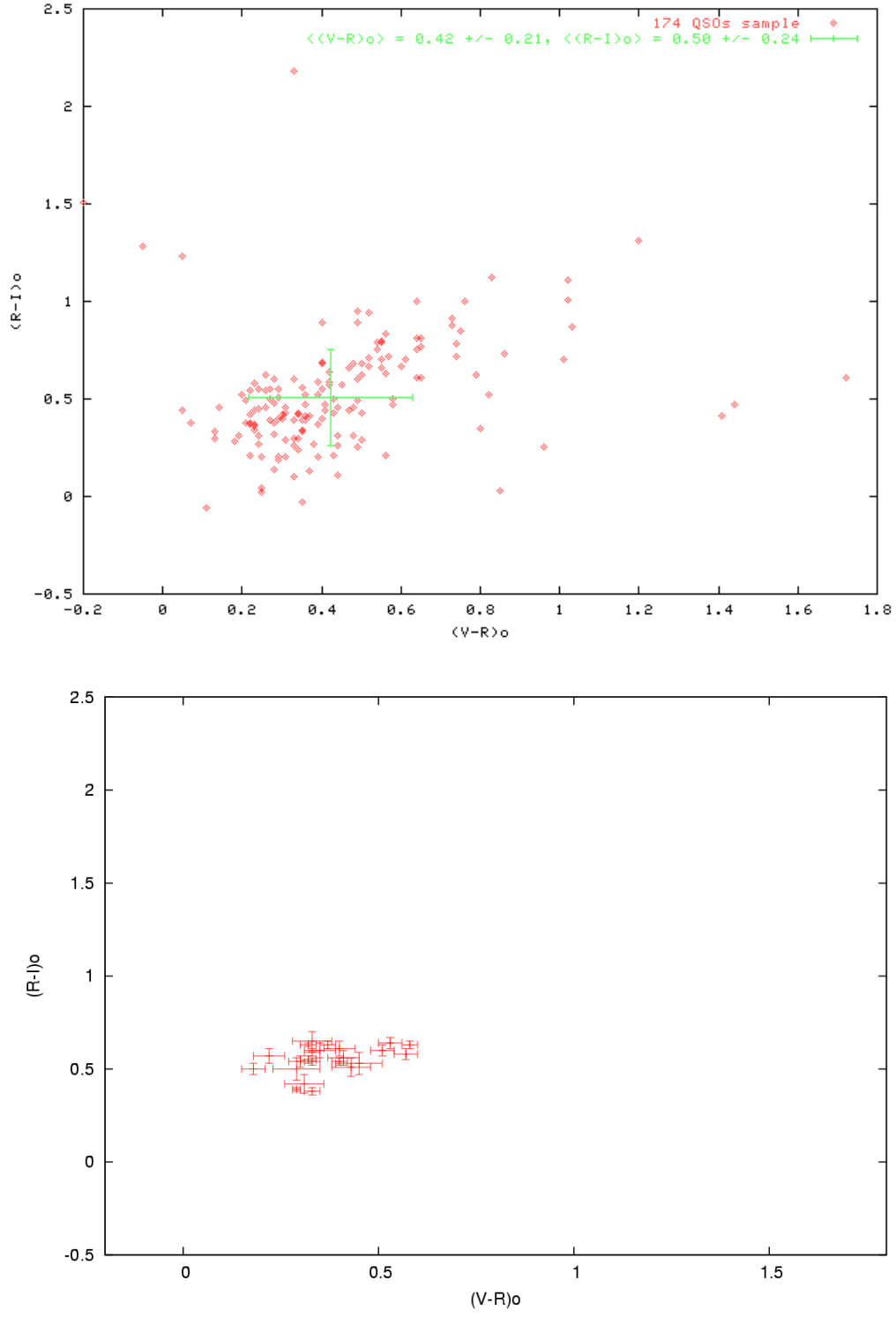

Figure 27: Comparison of $(R\text{-}I)_0$ vs. $(V\text{-}R)_0$ diagrams of AGN and blazars on a same scale. (*AGN data: Topinka* 2002)

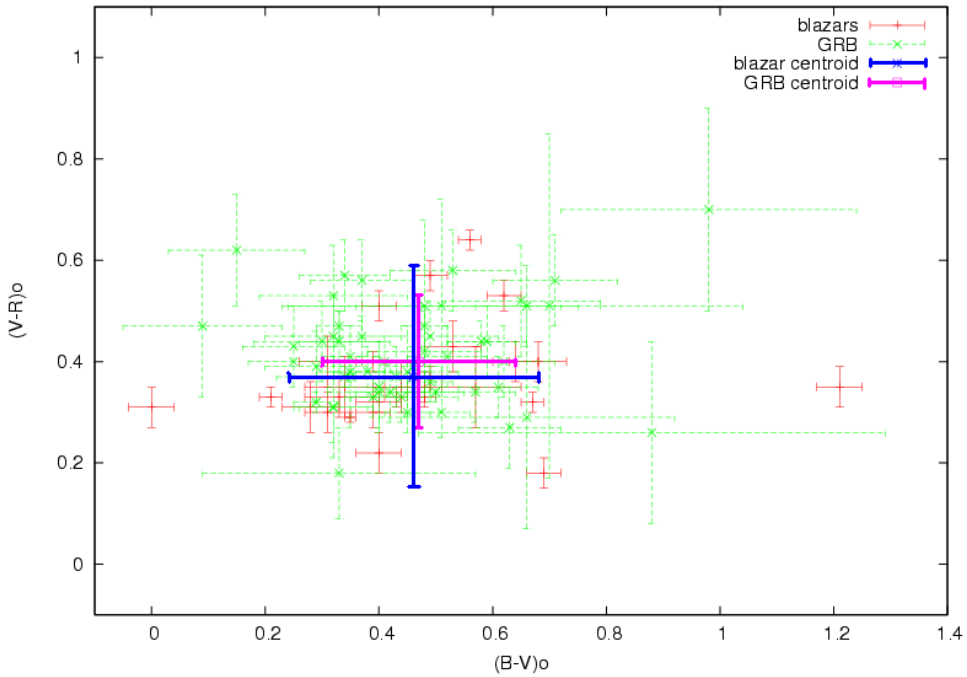

Figure 28: Positions of blazars, GRB and their centroids in $(V\text{-}R)_0$ vs. $(B\text{-}V)_0$ diagram.

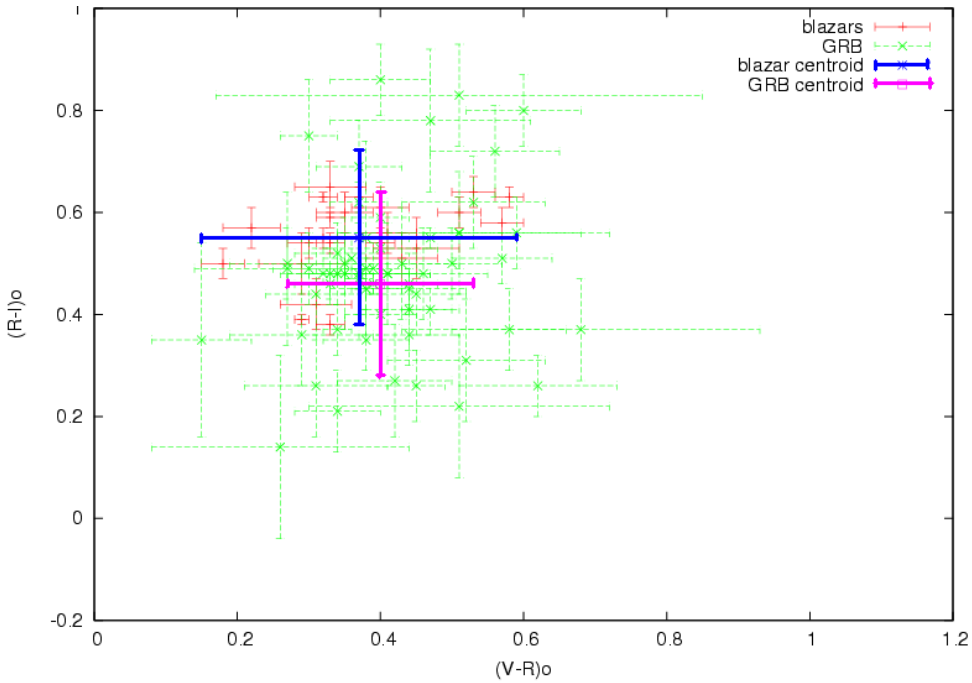

Figure 29: Positions of blazars, GRB and their centroids in $(R\text{-}I)_0$ vs. $(V\text{-}R)_0$ diagram.

5 Conclusions

Catalogues of optical monitoring of a sample of blazars gives us a large database and shed light on this intriguing class of astronomical objects. In our work we have analyzed the dereddened spectral flux distribution of 33 blazars. Such work can be used to map the optical spectral flux distribution, and to include our results within the overall SED of these objects.

A discussion based on our optical data alone gives some new implications for the existing theoretical models:

- Low-frequency peaked BL Lac objects are extremely variable in the optical region and their spectral slope clusters around $\alpha = 1.5$, in agreement with a Synchrotron Self-Compton model (Chiang&Bottcher 2002).

- The fact that the optical spectral slope of HBLs ranges from 0.8 to 2.2 may be the sign of a deformation of the SED for some of these sources. This deformation can be possible due to a thermal contribution to the overall optical signal, for example the host galaxy, or to non-thermal emission from different regions with respect to those that dominate the SED at higher frequencies.

Many of these blazars show a weak but general trend toward spectral slope flattening when the source is brighter. Our data alone are not enough to distinguish if this is sign of the presence of two or more components that contribute to the overall emission in the optical, or a typical feature of a single component synchrotron source. The same problem arises when we try to comment on our data for FSRQs. We analyze the overall emission coming from the source, and it is not easy to distinguish the thermal from the non-thermal components using optical data alone.

What we can try to do is to comment a consistency of our data with models of blazars presented in Section 3.3:

- We can exclude the interstellar scintillation as a phenomenon which would cause variability in the optical region of our dataset, since it only affects radio band of the SED.

- Gravitational lenses bend all frequencies equally so the flares caused by microlensing should be achromatic. Although some flares are thought to be caused by microlenses (see Section 3.3.2), we saw that general trend of blazar spectral slope is flattening with increasing brightness (i.e. during the flare) so we cannot accept microlensing as a significant effect causing variability of blazars.

- Accretion disk models are more plausible fro HBLs and FSRQs (for LBLs there is strong evidence for synchrotron radiation only) because

it is possible that when blazar is in quiescent state, the addition of the disk to the emission can be much greater than during the flare, when the jet emission outshines the disk. Therefore thermal emission from the disk might be a factor that disturbs SED of blazars.

- Geometrical effects surely play an important role in explaining variability of blazars, since their emission is extremely dependent on Doppler factor which changes with slight variations of direction of the jet. Also binary black holes in centers of blazars are commonly accepted phenomenon thus allowing geometrical effects to influence flux from blazars.

- Shock-in-jet model is also consistent with spectral flattening (or bluer-when-brighter tendency). To accept or reject this model we would need multispectral measurements of the sources, since as was explained, flare induced by the shock in jet would cause simultaneous increasing of flux at all frequencies, but peak of this flux would first occur at the highest frequencies and then "travel" through all wavelengths towards the radio band. However, optical region is so narrow that we cannot investigate any asynchrony in flux peaking in different filters.

We also examined color properties of our blazars, in analogy to the analogous analyses performed for OAs of GRBs, since colors can tell us much about environment around blazars and help us to identify blazars in all-sky surveys. From the dereddened (i.e. corrected for the Galactic extinction) color-color diagrams of our dataset and from comparison with other extragalactic objects we see how small is the scatter of blazars in these diagrams. This can indicate that there is very similar or no environment (apart from our Galaxy) on our line of sight to blazars. This in the latter case can mean that blazars, as well as optical afterglows of gamma-ray bursts, destroy dust with their strong X-ray emission.

The average color indices of blazars were found to be
$(B-V)_0 = 0.46 \pm 0.22$
$(V-R)_0 = 0.37 \pm 0.22$
$(R-I)_0 = 0.55 \pm 0.17$

This is very similar to those of OAs of GRBs. The similarity of mean colors of blazars and of OAs of GRBs we explain as similarity in physical processes generating the optical emission (synchrotron spectrum) which is consistent with recent understanding of both blazars as well as OAs of GRBs.

However interesting result which is now and in our opinion was unknown before is the fact that the scatter of color indices of sample of analyzed blazars is relatively very small, in analogy to the OAs of GRBs. This finding we explain as fact that there is almost no dust along the line of sight since the other explanation namely that the reddening is identical for all blazars studied is very improbable. As shown before for OAs of GRBs, the scatter

of color indices is hence an efficient tool to study the environment of the sources. Since the results for OAs of GRBs are usually explained by the fact that the dust has been destroyed by the energetic radiation of the GRB, we argue that the same is probably valid for blazars where the dust along the line of sight i.e. in the jet may be destroyed by the energetic blazar emission and/or that there is no material along the line of sight.

Another interesting finding is that the scatter in color diagram of AGNs is significantly larger than those of blazars. In our understanding this is caused by the fact that for AGNs, the line of sight is not consistent with the jet, hence the light is affected by the material surrounding the AGN. This is also consistent with the present understanding and scenario of AGN and blazars in general.

We have tried to use this similarity of average blazar colors for identifications in all-sky surveys, like SLOAN. And we found out that though blazar, OA of GRB and AGN average colors are too close to reliably distinguish among these objects, this group has a different position on color-color diagrams than other astronomical objects, like stars, supernovae, etc. Thus it could be possible to use colors of blazars to pick blazar candidates in optical surveys.

All this suggests a possible future prospects. The study described here has indicated the scientific value of color analyses in investigations of blazars. It is obvious that the continuation of these studies can yield another valuable results. Based on the experience from the recent study and from analogous analyses of another astrophysical objects, we propose to analyze larger sample of objects and to try to study in more details the color changes during the flares of blazars in order to understand the underlying physical processes. This will require detailed multicolor photometry of blazars during their flares which are almost unavailable recently. The color analyses can be also applied to Seyfert galaxies. We propose these analyses to be performed in future within the PhD program of the author of this thesis.

The analyses and studies described in this works have been performed in close collaboration with the Group of High Energy Astrophysics at the Astronomical Institute of the Academy of Sciences of the Czech Republic, Ondřejov. Some parts of the analyses were related to the projects coordinated by this group (grant A30003206 by the Grant Agency of the Academy of Sciences of the Czech Republic and ESA PECS project 98023).

References

[1] Abraham Z., Romero G. E., 1999, *A&A*, 344, 61

[2] Abramowicz M. A., et al., 1991, *A&A*, 245, 454

[3] Abramowicz M. A., et al., 1992, *Nature*, 356, 41

[4] Antonucci R., 1993, *ARAA*, 31, 473

[5] Bai J. M., et al., 1998, *A&A*, 132, 83

[6] Bai J. M., et al., 1999, *A&A*, 136, 455

[7] Barth A. J., et al., 2002, *ApJ*, 566, 13

[8] Barth A. J., et al., 2003, *ApJ*, 583, 134

[9] Begelman M. C., et al., 1980, *Nature*, 287, 307

[10] Belokon E. T., 1999, *AstL*, 25, 781B

[11] Bessel H. S., 1979, *PASP*, 91, 589

[12] Bian W., Zhao Y., 2004, *MNRAS*, 347, 607

[13] Bignall H. E., *ev. conf.*, 19B

[14] Blandford R. D., Znajek R. L., 1977, *MNRAS*, 179, 433

[15] Blandford R. D., Payne D. G., 1982, *MNRAS*, 199, 883

[16] Bondi M., et al., 2001, *MNRAS*, 325, 1109

[17] Camendzin M., Krockenberger M., 1992, *A&A*, 255, 59

[18] Cao X. W., 2002, *ApJ*, 570, 13

[19] Chakrabarti S. K., Wiita P. J., 1993, *ApJ*, 411, 602

[20] Chiang J., Bottcher M., 2002 *ApJ*, 564, 92

[21] Ciprini S., et al., 2003, *A&A*, 400, 487

[22] Ciprini S., et al., 2004, *MNRAS*, 348, 1379

[23] Clements S. D., et al., 2003, *AJ*, 126, 37

[24] Donato D., et al., 2001, *A&AS*, 375, 739

[25] Donea A. C., Biermann P. L., 2002, *PASA*, 19, 125

[26] Fan J. H., et al., 1997, *A&AS*, 125, 525

[27] Fan J. H., et al., 1998, *ApJ*, 507, 173

[28] Fan J. H., et al., 1999, *ApJS*, 121, 131

[29] Fan J. H., Lin R. G., 2000a, *ApJ*, 537, 101

[30] Fan J. H., Lin R. G., 2000b, *A&A*, 355, 880

[31] Fan J. H., et al., 2001a, *ChJA&A*, 25, 282

[32] Fan J. H., et al., 2002, *A&A*, 381, 1

[33] Fan J. H., et al., 2004, *ChJA&A*, 4, 133

[34] Fan J. H., 2005, *ChJAA*, 5, 213

[35] Fan J. H., et al., *gra conf.*, 291

[36] Fiorucci M., et al., 1996, *A&A*, 117, 475

[37] Gay-Yam A., et al., 2004, *PASP*, 116, 597

[38] Ghisellini G., Madau P., 1996, *MNRAS*, 280, 67

[39] Ghisellini G., Maraschi L., 1996, San Francisco *ASP*, 436

[40] Guibin J., et al., 1995, *A&A*, 114, 337

[41] Guibin J., et al., 1998, *A&A*, 128, 315

[42] Heuge T., Falcke H., *Principles of synchrotron emission in an astrophysical context*, lecture notes, http://www-ik.fzk.de/huege/downloads/synchrotronprinciples.pdf

[43] Hioruchi T., Kato S., 1990, *PASJ*, 42, 661

[44] Hudec R., in *Gamma-Ray Bursts - 5th Huntsville Symposium*, ed. R. M. Kippen, R. S. Mallozzi, & G. J. Fishman, AIP Conf. Proc., 526

[45] Hughes P. A., et al., 1985, *ApJ*, 298, 301

[46] Jurkevich I., 1971, *Ap&SS*, 13, 154

[47] Karas V., *Astrophysical Analogies: From quasars to pulsars*, 1996

[48] Kayser R., 1988, *A&A*, 206, L8

[49] Kellermann K. I., et al., 1989, *AJ*, 98, 1195

[50] Kinman T. D., 1975, *IAUS*, 67, 573

[51] Kollgaard R. I., et al., 1994, *New York: AIP*

[52] Komossa S., et al., 2003, *ApJL*, 582, 15

[53] Kranich D., et al., 1999, *astro-ph*/9907205

[54] Krishan V., Wiita P. J., 1994, *ApJ*, 423, 172

[55] Lainela M., et al., 1999, *ApJ*, 521, 561

[56] Lawrence A., Papadakis I., 1993, *ApJ*, 414, L85

[57] Liang E. W., Liu H. T., 2003, *MNRAS*, 340, 63

[58] Liu F. K., et al., 1995, *A&A*, 295, 1

[59] Managalam A. V., Wiita P. J., 1993, *ApJ*, 406, 420

[60] Mao L., et al., 2005, *ChJAA*, 5, 471

[61] Maraschi L., Tavecchio F., 2003, *ApJ*, 593, 667

[62] Marscher A. P., Travis J. P., 1991, *Variability of Blazars*, ed. Valtaoja&Valtonen (Cambridge Univ. Press), 153

[63] Massaro E., Trévese D., 1996, *A&A*, 312, 810

[64] Meyer F., Meyer-Hofmeister E., 1984, *A&A*, 132, 143

[65] Mineshige S., et al., 1994, *Pub. Astr. Soc. Japan*, 46, 97

[66] Paczynski B., 1986, *ApJ*, 301, 503

[67] Padovani P., Giommi P., 1995, *ApJ*, 444, 567

[68] Padovani P., 2003, *ChJAA*, 3S, 147P

[69] Perlman E. S., et al., 1998, *AJ*, 115, 1253

[70] Pian E., et al., 1998, *ApJ*, 492, L17

[71] Pursimo T., et al., 2000, *A&AS*, 146, 141

[72] Raiteri C. M., et al., 1998, *A&A*, 127, 445

[73] Raiteri C. M., et al., 2001, *A&A*, 377, 396

[74] Rieger F. M., Mannheim K., 2000, *A&A*, 359, 948

[75] Rieger F. M., Mannheim K., 2003, *A&A*, 397, 121

[76] Rieger F. M., 20004, *in 5th Microquasar Workshop, Beijing*

[77] Romero G. E., et al., 2000, *AJ*, 120, 1192

[78] Sagar R., et al. 1996, *MNRAS*, 281, 1267

[79] Sambruna R., et al., 1996, *ApJ*, 463, 444

[80] Schramm K. J., et al., 1993, *A&A*, 278, 391

[81] Sillanpaa A., et al., 1988, *ApJ*, 325, 628

[82] Sillanpaa A., et al., 1996a, *A&A*, 305, L17

[83] Sillanpaa A., et al., 1996b, *A&A*, 305, L13

[84] Smith A. G., Nair A. D., 1995, *PASP*, 107, 863S

[85] Šimon V., et al., 2001, *A&A*, 377, 450

[86] Šimon V., et al., 2004, *A&A*, 427, 901

[87] Šimon V., eta l., 2005, *Baltic Astronomy*, 13, 253

[88] Takahashi T., et al., 1996, *ApJ*, 470, L89

[89] Takalo L. O., et al., 1999, *BL Lac Phenomenon*, p. 253

[90] Telting J. H., et al., 1998, *MNRAS*, 296, 785

[91] Terrell J., Olsen K. H., 1972, *IAUS*, 44, 179

[92] Topinka M., 2002, *Diploma thesis*, MFF UK Prague

[93] Tosti G., et al., 1999, *ASP Conf. Ser. Vol.* 159, p. 145

[94] Urry C. M., Padovani P., 1995, *PASP*, 107, 803

[95] Urry C. M., 1996, *ASPC*, 110, 391U

[96] Urry C. M., et al., 1997, *ApJ*, 486, 799

[97] Villata M., et al., 1997, *A&A*, 121, 119

[98] Villata M., Raiteri C. M., et al., 1998, *MNRAS*, 293, L13

[99] Villata M., Raiteri C. M., 1999, *A&A*, 347, 30

[100] Villata M., et al., 2000, *A&A*, 144, 481

[101] Wagner S. J., Witzel A., 1995, *ARA&A*, 33, 163

[102] Wagner S. J., et al., 1995, *A&A*, 298, 688W

[103] Waxman E., Draine B. T., 2000, *ApJ*, 537, 796

[104] Webb, J. R., et al., 2000, *AJ*, 120, 41

[105] Wiita P. J., Xiong Y., 1997, *Theory of Black Hole Accretion Disks*, Abramowicz M. A., et al. eds., Cambridge University press, Cambridge, in press

[106] Woo J. H., Urry C. M., 2003, *ApJ*, 583, 47

[107] Wu W.-B., et al., 2002, *A&A*, 389, 742

[108] Xie G. Z., et al., 1994, *A&A*, 106, 361

[109] Xie G. Z., et al., 1999, *ApJ*, 522, 846